HHS Public Access

Author manuscript

Nature. Author manuscript; available in PMC 2021 April 28.

Published in final edited form as:

Nature. 2020 November ; 587(7833): 258–263. doi:10.1038/s41586-020-2860-1.

Parallel ascending spinal pathways for affective touch and pain

Seungwon Choi[1], **Junichi Hachisuka**[2,5], **Matthew A. Brett**[1], **Alexandra Magee**[1], **Yu Omori**[2,6], **Noor-ul-Aine Iqbal**[1], **Dawei Zhang**[1], **Michelle M. DeLisle**[1], **Rachel L. Wolfson**[1], **Ling Bai**[1], **Celine Santiago**[1], **Shiaoching Gong**[3], **Martyn Goulding**[4], **Nathaniel Heintz**[3], **H. Richard Koerber**[2], **Sarah E. Ross**[2], **David D. Ginty**[1,*]

[1]Department of Neurobiology, Howard Hughes Medical Institute, Harvard Medical School, 220 Longwood Avenue, Boston, MA 02115, USA

[2]Department of Neurobiology and the Pittsburgh Center for Pain Research, University of Pittsburgh, Pittsburgh, PA 15213, USA

[3]The Laboratory of Molecular Biology, Howard Hughes Medical Institute, The Rockefeller University, New York, NY 10065, USA

[4]Molecular Neurobiology Laboratory, The Salk Institute for Biological Studies, 10010 North Torrey Pines Road, La Jolla, CA 92037, USA

[5]Current address: Institute of Neuroscience and Psychology, Sir James Black Building, University of Glasgow, University Avenue, Glasgow G12 8QQ, United Kingdom

[6]Current address: Toray Industries, Inc., Pharmaceutical Research Laboratories,10-1, Tebiro 6-chome, Kamakura, Kanagawa 248-8555, Japan

Summary

The anterolateral pathway consists of ascending spinal tracts that convey pain, temperature and touch information from the spinal cord to the brain[1–4]. Projection neurons (PNs) of the anterolateral pathway are attractive therapeutic targets for pain treatment because nociceptive signals emanating from the periphery channel through these spinal PNs *en route* to the brain. However, the organizational logic of the anterolateral pathway remains elusive. Here, we show that two PN populations that express structurally related GPCRs, TACR1 and GPR83, form parallel ascending circuit modules that cooperate to convey tactile, thermal and noxious cutaneous signals from the spinal cord to the lateral parabrachial nucleus of the pons (PBN_L). Axons of *Tacr1*- and *Gpr83*-expressing spinoparabrachial (SPB) neurons innervate distinct sets of PBN_L subnuclei, and

*correspondence: david_ginty@hms.harvard.edu.

Author contributions

S.C. and D.D.G. conceived and designed the project. S.C. screened and characterized the new anterolateral pathway PN mouse lines, and designed, executed and analyzed the histology, behavior, and spinal cord slice recording experiments. M.A.B., A.M. and N.I. assisted in executing and analyzing histology and behavioral experiments. D.Z. assisted in RNAscope analyses. M.M.D. and R.L.W. assisted in executing and analyzing behavioral experiments. The *ex vivo* spinal cord physiological recordings were done by J.H., Y.O. and S.C, and analyzed by J.H., Y.O., S.E.R., and H.R.K. N.H. and S.G. generated the *Calca-FlpE* BAC transgenic mouse line. L.B. characterized *Calca-FlpE* and *Advillin*^{FlpO} mouse lines, and C.S. characterized *Tau*^{FSFiAP} mouse line. M.G. provided the *Lbx1*^{FlpO} mouse line. S.C. and D.D.G. wrote the manuscript with input from all authors.

Competing interests

The authors declare no competing interests.

strong optogenetic stimulation of their axon terminals induces distinct escape behaviors and autonomic responses. Moreover, *Gpr83*-expressing SPB neurons are highly sensitive to cutaneous mechanical stimuli and receive strong synaptic inputs from both high- and low-threshold primary mechanosensory neurons. Remarkably, the valence associated with activation of *Gpr83*-expressing SPB neurons is either positive or negative depending on stimulus intensity. These findings reveal anatomically, physiologically, and functionally distinct SPB tract subdivisions that underlie affective aspects of touch and pain.

While primary sensory neurons that respond to a range of innocuous or noxious stimuli acting on the skin have been identified and characterized[1,2,5], less is known about how their signals are integrated and processed within the spinal cord and conveyed via spinal PNs to the brain to underlie somatosensory perception and behavior. Here, we sought to generate mouse genetic tools for spinal cord anterolateral pathway PNs and use them for anatomical, electrophysiological, and behavioral analyses to define ascending pathways that underlie affective touch and pain.

Genetically defined spinal PN subsets

We generated a *Tacr1*^{CreERT2} knockin mouse line (Fig. 1a, Extended Data Fig. 1a2, b1–3) and found that *Tacr1*$^{+}$ SPB neurons are *Gad2*-negative and represent a large subset (57.3 ± 4.7%) of the total SPB population (Extended Data Fig. 2a, b, e, f), as previously reported[3,6]. In addition, to identify other, novel subsets of SPB neurons, we conducted an *in silico* screen of BAC-GFP transgenic mouse lines from the GENSAT project[7]. One of these lines, *Gpr83-GFP*, was found to label a major subset of SPB neurons (52.7 ± 4.4% of the total SPB population) (Fig. 1b). In addition, a newly generated *Gpr83*^{CreERT2} knockin mouse line labels PNs of the anterolateral pathway that are *Gad2*-negative and account for 45.2 ± 2.4% of SPB neurons (Extended Data Fig. 1a3, c, 2a, b, e, f). Further analysis revealed that the *Gpr83*$^{+}$ and *Tacr1*$^{+}$ SPB populations are numerically comparable, largely non-overlapping, and together account for the majority (88.4 ± 2.7%) of SPB neurons in spinal cord lamina I +IIo (Fig. 1f–h, Extended Data Fig. 2e–g). *Tac1*$^{+}$ SPB neurons, a previously reported SPB population[8], account for 22.1 ± 3.4% of SPB neurons in lamina I+IIo, and *Tac1* is expressed in subsets of both *Tacr1*$^{+}$ and *Gpr83*$^{+}$ SPB neurons (38.2 ± 4.0% and 47.8 ± 9.7%, respectively), suggesting that *Tac1*$^{+}$ SPB neurons may represent the small subset of SPB neurons that express both *Tacr1* and *Gpr83* (Extended Data Fig. 2j–n). We also generated a *Robo3*$^{IRES\text{-}CreERT2}$ knockin mouse line (Extended Data Fig. 1a1) because Robo3 is transiently expressed in developing commissural neurons[9], including PNs of the anterolateral pathway.

To define brain targets of anterolateral pathway PNs, we visualized axonal projections of *Tacr1*$^{+}$, *Gpr83*$^{+}$, or *Robo3*$^{+}$ spinal PNs to the brain using intersectional genetic strategies (PN Cre; *Lbx1*$^{FlpO\ 10}$ (or *Cdx2-NSE-FlpO*[11]); *Rosa26*$^{FSF\text{-}LSL\text{-}tdTomato}$). We observed that the PBN_L is the most densely innervated brain region for both *Tacr1*$^{+}$ and *Gpr83*$^{+}$ spinal PNs (Fig. 1c, d, e). In the thalamus, medial and posterior thalamic nuclei are innervated by both *Tacr1*$^{+}$ and *Gpr83*$^{+}$ spinal PNs in a partially overlapping manner (Fig. 1c, d). In contrast, the ventral posterolateral nucleus of the thalamus (VPL) is innervated by *Robo3*$^{+}$

spinal PNs (Extended Data Fig. 1d). In the midbrain, both *Tacr1*$^+$ and *Gpr83*$^+$ spinal PNs innervate the lateral region of the periaqueductal grey (PAG) and the midbrain reticular nucleus (MRN), while *Tacr1*$^+$ spinal PNs more densely innervate the superior colliculus with a compartmentalized array of terminal patches in the intermediate grey layer (SCig) (Fig. 1c, d). In the brainstem, both *Tacr1*$^+$ and *Gpr83*$^+$ PNs innervate the medial accessory olive (MAO) and the lateral reticular nucleus (LRN), while *Gpr83*$^+$ PNs uniquely innervate the dorsal fold of the dorsal accessory olive (DAOdf) (Extended Data Fig. 2h, i). Anatomical analyses using a dual-virus labeling approach (Extended Data Fig. 3) revealed that axons of both *Tacr1*$^+$ and *Gpr83*$^+$ posterior thalamus-projecting neurons travel through the ventral lateral funiculus of the spinal cord white matter and form collateral branches that terminate in the MAO and LRN of the ventral brainstem. In contrast, axons of *Tacr1*$^+$ SCig-projecting neurons travel through the dorsal lateral funiculus and form collateral branches that terminate in the PAG. Strikingly, none of these thalamic- and midbrain-projecting *Tacr1*$^+$ or *Gpr83*$^+$ PNs formed collateral branches terminating within the PBN_L, the most densely innervated brain target of anterolateral pathway PNs. These findings indicate that *Tacr1*$^+$ and *Gpr83*$^+$ spinal PNs that innervate the posterior thalamus, midbrain, and PBN_L are distinct populations.

Zonal segregation of SPB axon terminals

The PBN_L is comprised of several cytoarchitecturally distinct subnuclei that have distinct input/output connections with other brain regions[12,13]. We found that the axons of spinal PNs, labeled in their entirety using *Cdx2-Cre*; *Rosa26*$^{LSL\text{-}synaptophysin\text{-}tdTomato}$ mice, terminate within all PBN_L subnuclei, except for the ventrolateral subnucleus (PBN_{VL}) and the center region of the external lateral subnucleus (PBN_{EL}) (Fig. 2a). Whereas *Tacr1*$^+$ SPB neurons form synapses mainly within the central lateral (PBN_{CL}) and internal lateral (PBN_{IL}) subnuclei, *Gpr83*$^+$ SPB neurons form synapses uniquely within the dorsal lateral (PBN_{DL}) and PBN_{EL} subnuclei, in addition to the PBN_{IL} (Fig. 2b, c, d). Accordingly, presynaptic terminals of *Gpr83*$^+$ SPB neurons are associated with $CGRP^+$ neurons within the PBN_{EL}[14], whereas *Tacr1*$^+$ axon terminals are not (Extended Data Fig. 4a, b). Moreover, *Tac1*$^+$ SPB neurons form synapses only within the PBN_{IL} (Extended Data Fig. 2o–q), which is the sole PBN_L subnucleus receiving both *Tacr1*$^+$ and *Gpr83*$^+$ SPB synaptic terminals (Fig. 2c, d). Thus, distinct SPB populations form synaptic terminals within the PBN_L in a zonally segregated manner.

The finding that *Tacr1*$^+$ and *Gpr83*$^+$ SPB neurons innervate distinct sets of PBN_L subnuclei led us to hypothesize that these two SPB populations underlie distinct behavioral responses to somatosensory stimuli. Selective, bilateral optogenetic activation of either *Tacr1*$^+$ or *Gpr83*$^+$ SPB neuron axon terminals within the PBN_L (Fig. 2e) strongly induced the expression of the immediate early gene Fos in the respective PBN_L subnuclei (Fig. 2f, g) predicted by the synaptic terminal analysis (Fig. 2b, c, d). Interestingly, strong stimulation of *Tacr1*$^+$ axon terminals also resulted in Fos expression in the PBN_{EL}, in addition to the PBN_{CL} and PBN_{IL} (Fig. 2f, g), consistent with the presence of local microcircuits that interconnect these PBN_L subnuclei[15]. Behaviorally, high-power (6.5 mW) optogenetic stimulation of either *Tacr1*$^+$ or *Gpr83*$^+$ SPB neuron terminals led to a robust increase in locomotion in a time-locked manner (Fig. 2h, i), reminiscent of escape behaviors observed

in response to noxious stimuli. Interestingly, while *Gpr83*$^+$ terminal stimulation promoted forward locomotion, *Tacr1*$^+$ terminal stimulation induced a pronounced backward "retreat" behavior as well as jumping (Fig. 2j, Extended Data Fig. 4d–f, Supplementary Video 1–3). Both light-activated hyperlocomotion and jumping were abolished following infusion of the glutamatergic synaptic blocker NBQX into the PBN_L (Fig. 2k, l), and Fos induction was not observed in the spinal cord following photostimulation of SPB axon terminals (Extended Data Fig. 4g, h), suggesting that escape behaviors evoked by SPB axon terminal stimulation is mediated by glutamatergic synaptic transmission within the PBN_L and not by backpropagating action potentials and activation of other brain regions or the spinal cord. It is noteworthy that light-evoked increases in locomotion were followed by a robust "freezing" behavior that lasted for the entire light-off period (Extended Data Fig. 4c, Supplementary Video 4). Moreover, activation of either *Tacr1*$^+$ or *Gpr83*$^+$ SPB neurons led to an increase in pupil diameter (Fig. 2m, n), which likely reflects increased sympathetic tone. While pupillary dilation evoked by *Gpr83*$^+$ SPB terminal stimulation was transient (fast decay and small area under curve), dilation evoked by *Tacr1*$^+$ SPB terminal stimulation was sustained (Fig. 2m, o). *Tacr1*$^+$ SPB terminal stimulation additionally induced squinting/blinking, indicative of severe pain[16] (Fig. 2m, p). These findings suggest that high-intensity stimulation of *Tacr1*$^+$ and *Gpr83*$^+$ SPB neurons induces nocifensive behaviors, but these two SPB populations differentially influence the mode of escape locomotor behavior and the temporal dynamics of autonomic responses.

A mechanosensory limb of the SPB pathway

PNs of the anterolateral pathway are heterogeneous in terms of their physiological response properties, and the majority are polymodal[3,17–20]. To determine the response properties of *Gpr83*$^+$ and *Tacr1*$^+$ SPB subsets, we conducted whole-cell patch-clamp recordings from these two neuronal populations using an *ex vivo* skin-spinal cord preparation[18] (Fig. 3a). Despite heterogeneity in the tuning properties among individual *Gpr83*$^+$ and *Tacr1*$^+$ SPB neurons, *Gpr83*$^+$ and *Tacr1*$^+$ SPB subsets at the population level exhibited distinct responses to mechanical and thermal stimuli (Fig. 3b–g, Extended Data Fig. 5a, b); *Gpr83*$^+$ SPB neurons were highly sensitive to mechanical stimuli (Fig. 3e), whereas *Tacr1*$^+$ SPB neurons were more responsive to innocuous thermal stimuli, cool temperature (15°C) in particular, and capsaicin than *Gpr83*$^+$ SPB neurons (Fig. 3f, Extended Data Fig. 5c, d). Interestingly, *Gpr83*$^+$ and *Tacr1*$^+$ SPB neurons both responded to noxious cold (0°C) and noxious heat (54°C) (Fig. 3g), suggesting that both of these SPB subdivisions convey noxious thermal signals.

Consistent with these *ex vivo* recordings, extensive paw-licking, a nocifensive behavior, elicited by noxious heat (55°C) or noxious cold (5°C) and reactivity to noxious mechanical stimuli as well as rough floor aversion were diminished when neurotransmission was suppressed in both *Gpr83*$^+$ and *Tacr1*$^+$ spinal neurons, including SPB neurons, simultaneously but not when neurotransmission was suppressed in either *Gpr83*$^+$ or *Tacr1*$^+$ spinal neurons alone (Extended Data Fig. 6). Together, these physiological and behavioral findings suggest that *Gpr83*$^+$ and *Tacr1*$^+$ SPB populations differentially transmit innocuous cutaneous signals to the brain, while noxious tactile and thermal signals are conveyed by both SPB subdivisions.

To define spinal cord circuit mechanisms that account for differences in stimulus-response properties of *Tacr1*$^+$ and *Gpr83*$^+$ SPB neurons, we next examined the sensory neuron inputs onto these SPB neurons using channelrhodopsin-assisted circuit mapping in acute spinal cord slices (Fig. 3h). Photostimulation (473 nm) of CGRP$^+$ peptidergic nociceptor terminals, labeled using a newly generated BAC transgenic mouse line, *Calca-FlpE* (Extended Data Fig. 1f), evoked large EPSCs and action potential firing in most *Tacr1*$^+$ SPB neurons, but not in *Gpr83*$^+$ SPB neurons (Fig. 3j, k) except for a small fraction that exhibited small polysynaptic EPSCs evoked with much longer light pulses (Extended Data Fig. 7b). In contrast, activation of either *Mrgprb4*$^+$ mechanosensory neuron[21] terminals or *Ntrk2*$^+$ (also known as *TrkB*) Aδ-low threshold mechanoreceptor (LTMR)[22] terminals evoked large EPSCs and action potential firing in the majority of *Gpr83*$^+$ SPB neurons, but not in *Tacr1*$^+$ SPB neurons (Fig. 3l–o) except for a small fraction that exhibited small polysynaptic EPSCs evoked with much longer light pulses (Extended Data Fig. 7c, d). Activation of *Mrgprd*$^+$ polymodal non-peptidergic sensory neuron[23] terminals evoked large EPSCs and action potential firing in both *Gpr83*$^+$ and *Tacr1*$^+$ SPB neurons (Extended Data Fig. 7e, f). A morphological correlate of the differential sensory neuron inputs is that dendrites of *Tacr1*$^+$ SPB neurons are restricted to the most superficial spinal cord lamina, where most CGRP$^+$ peptidergic nociceptors terminate, whereas dendrites of *Gpr83*$^+$ SPB neurons often extend into lamina IIid, the site of non-peptidergic sensory neuron synapses, including those of *Mrgprb4*$^+$ mechanosensory neurons, and even into lamina IIiv and III, the site of Aδ-LTMR and Aβ-LTMR synapses (Extended Data Fig. 7g–k). Thus, the distinct physiological responses of *Gpr83*$^+$ and *Tacr1*$^+$ SPB neurons to tactile and thermal stimuli can be explained by differences in their dendritic morphologies and synaptic inputs from distinct classes of mechanosensory neurons and nociceptors.

SPB neuronal subsets and hedonic value

Several lines of evidence indicate that the organizational properties of the *Gpr83*$^+$ and *Tacr1*$^+$ SPB subdivisions are distinct from other ascending pathways of anterolateral spinal tracts. First, in contrast to other brain targets, including the PAG and SCig, which are innervated by axons originating exclusively from the contralateral side of the spinal cord, the PBN_L was found to receive bilateral input from both *Gpr83*$^+$ and *Tacr1*$^+$ SPB neurons (Fig. 4a, b). Simultaneous retrograde tracing of SPB neurons innervating either side of the PBN_L (Extended Data Fig. 8a–c) and anterograde tracing of sparsely labeled SPB axons (Fig. 4c–f) revealed that individual SPB neurons project either contralaterally, ipsilaterally, or bilaterally. Second, consistent with our observations from dual-virus retrograde labeling experiments (Extended Data Fig. 3), single axon tracing analyses of sparsely labeled *Gpr83*$^+$ and *Tacr1*$^+$ SPB neurons support the idea that most SPB neurons are dedicated anterolateral pathway PNs that innervate the PBN_L without forming collateral branches that innervate other brain regions (Fig. 4e). In contrast, anterolateral pathway PNs with axons innervating the inferior olivary complex have collateral branches that extend to other brain regions (Extended Data Fig. 3f, i, 8d, e). Third, unlike other brain targets of the anterolateral pathway, such as the inferior olivary complex (Extended Data Fig. 8f), we observed no somatotopic organization of SPB axon terminals within the PBN_L (Fig. 4g–i).

These unique anatomical features led us to suspect that the *Tacr1*$^{+}$ and *Gpr83*$^{+}$ SPB subdivisions contribute to affective, rather than discriminative aspects of somatosensation. Consistent with this idea, activation of SPB neurons with moderate-intensity stimulation (1 mW), particularly *Tacr1*$^{+}$ SPB neurons, induced robust, repetitive grooming of forepaw and head (Extended Data Fig. 9a, b, Supplementary Video 5), which in rodents is a hallmark feature of stress and anxiety[24]. Selective activation of SPB axon terminals originating exclusively from the lumbar spinal cord also induced this rostral grooming behavior, but not grooming of body trunk, hindpaw, or tail (Extended Data Fig. 9c, d), consistent with the idea that the SPB pathways lack somatotopic organization. Moreover, high-intensity photostimulation (6.5 mW) of either *Tacr1*$^{+}$ or *Gpr83*$^{+}$ SPB axon terminals within the PBN_L induced strong place aversion (Fig. 5a, b). Interestingly, the aversive effect of high-intensity photostimulation of *Gpr83*$^{+}$ SPB neurons was transient and lasted only for the stimulation period, whereas activation of *Tacr1*$^{+}$ SPB neurons led to a sustained aversive behavior that continued after the stimulation period had ended, suggesting that strong activation of SPB neurons, particularly *Tacr1*$^{+}$ SPB neurons, evokes behaviors associated with negative emotional valence.

In addition to negative valence associated with noxious stimuli, observations in human patients with anterolateral cordotomy have implicated the anterolateral pathway in conveying signals associated with positive valence and pleasurable properties of gentle touch[25–27]. Our finding that *Gpr83*$^{+}$ SPB neurons are much more responsive than *Tacr1*$^{+}$ SPB neurons to light mechanical forces acting on the skin and receive strong synaptic inputs from mechanosensory neurons, including LTMRs, prompted us to ask whether *Gpr83*$^{+}$ SPB neurons convey signals that underlie positive valence associated with light touch as well as negative valence associated with noxious stimuli. To address this, we developed an optogenetic stimulation-coupled instrumental conditioning assay in which mice receive selective optogenetic stimulation of either *Tacr1*$^{+}$ or *Gpr83*$^{+}$ SPB axon terminals in the PBN_L upon pressing an active lever, but not an inactive lever (Fig. 5d). Remarkably, low-intensity, self-administered photostimulation (0.4 mW) of *Gpr83*$^{+}$ SPB neurons, but not *Tacr1*$^{+}$ SPB neurons, promoted positive reinforcement (i.e. increased lever-pressing) over time, whereas moderate-intensity photostimulation (1 mW) of either *Tacr1*$^{+}$ or *Gpr83*$^{+}$ SPB neurons served as a punishment signal (i.e. decreased lever-pressing) (Fig. 5e, f, Extended Data Fig. 9e, f). Interestingly, elevated lever-pressing and positive reinforcement associated with weak optogenetic stimulation of *Gpr83*$^{+}$ SPB neurons was observed for several days after photostimulation was uncoupled from pressing the active lever. Similarly, in a real-time place preference paradigm, only *Gpr83*^{CreERT2}; *Lbx1*^{FlpO}; *Rosa26*$^{LSL\text{-}FSF\text{-}ReaChR}$ mice exhibited preference for the stimulated side of the chamber following the period of moderate-intensity photostimulation (1 mW), but not strong photostimulation (6.5 mW) (Fig. 5b, c).

To begin to define cellular and circuit level correlates of intensity-dependent changes in behaviors associated with different valences (positive or negative), we next examined Fos induction in the PBN_L following photostimulation of SPB axon terminals with different optical strengths. High-intensity photostimulation (6.5 mW) of *Gpr83*$^{+}$ SPB axons terminals resulted in strong Fos induction in all three PBN_L subnuclei in which *Gpr83*$^{+}$ SPB axons terminals are associated, whereas low-intensity photostimulation (0.4 mW) induced Fos

expression only in the PBN_{EL} (Fig. 5g, h). Moreover, the number of Fos^+ neurons within the PBN_{EL}, including a Fos and CGRP double-positive population, correlated with stimulation intensity (Fig. 5h–j), suggesting that neurons within the PBN_{EL} may control behaviors associated with different valences in a scalable manner. Together, these findings indicate that the *Gpr83*$^+$ mechanosensory limb of the SPB tract is associated with either positive or negative emotional valence, depending on stimulus intensity.

Discussion

While studies of the anterolateral pathway have mainly focused on its role in pain and temperature sensation, subdivisions of the anterolateral pathway that may mediate affective touch have been poorly understood. We propose that the *Gpr83*$^+$ SPB pathway is a unique subdivision of the anterolateral pathway that conveys tactile information to higher brain centers via the PBN_L to underlie affective touch (Extended Data Fig. 10a). Support for this model includes the observations that *Gpr83*$^+$ SPB neurons are highly sensitive to mechanical stimuli, they receive strong synaptic inputs from primary mechanosensory neurons, and they convey tactile information bilaterally to the PBN_L in a manner that is non-topographically organized. In addition, low-intensity stimulation of *Gpr83*$^+$ SPB neurons is appetitive, whereas high-intensity stimulation of these neurons is aversive. It is noteworthy that *Gpr83*$^+$ SPB neurons receive synaptic inputs from both LTMRs and HTMRs, suggesting that the *Gpr83*$^+$ SPB pathway underlies either positive or negative valence associated with cutaneous mechanosensation depending on the properties or intensity of a tactile stimulus.

The current view of ascending pain pathways emphasizes the involvement of *Tacr1*$^+$ PNs in transmitting nociceptive signals from the spinal cord to the brain. However, therapeutic strategies that target *Tacr1*-expressing neurons and the TACR1 receptor itself to treat pain have been minimally successful[28], consistent with the existence of additional, *Tacr1*-negative SPB neurons[29]. Our physiological and behavioral findings suggest that *Tacr1*$^+$ and *Gpr83*$^+$ SPB neurons form parallel ascending circuit motifs that cooperate to convey nociceptive signals to the brain (Extended Data Fig. 10a). These two SPB modules receive synaptic inputs from distinct but overlapping sets of nociceptors and project to distinct but overlapping PBN_L subnuclei, which presumably engage different downstream brain regions associated with processing nociceptive signals. Indeed, strong activation of *Tacr1*$^+$ and *Gpr83*$^+$ SPB neurons generates spatiotemporally distinct patterns of escape locomotion, autonomic (pupillary) reactions, and place aversion, supporting the idea that these two SPB circuit motifs mediate different aspects of pain perception and behavioral responses to noxious stimuli. Intriguingly, TACR1 and GPR83 are structurally highly related GPCR family members (Extended Data Fig. 10b), both coupled to G_q signaling pathways[30], suggesting that they may modulate the activities of *Tacr1*$^+$ and *Gpr83*$^+$ SPB neurons, respectively. Future studies of the TACR1 and GPR83 GPCRs, and the spinal PNs that express them, may reveal new therapeutic approaches for treating disorders associated with pain and affective touch.

Methods

Mice.

Mice were handled and housed in accordance with Harvard Medical School and IACUC guidelines. Mice were kept in a temperature- and humidity-controlled room with a 12-hour light/dark cycle. Mice (2–24 weeks of age) from both genders were used in experiments. Knockin mouse lines generated in this study include the *Robo3*$^{IRES\text{-}CreERT2}$, *Tacr1*^{CreERT2}, *Gpr83*^{CreERT2}, *Advillin*^{FlpO}, and *Tau*^{FSFiAP} (this mouse line will be described elsewhere) mouse lines. These knockin mouse lines were generated in the Janelia Research Campus Gene Targeting and Transgenic Facility using conventional ES cell targeting strategies. Briefly, a 3X-STOP-IRES-CreERT2 cassette was introduced via homologous recombination into the first common coding exon that is shared by different splice variants of the *Robo3* gene for the *Robo3* $^{IRES\text{-}CreERT2}$ knockin mouse line. CreERT2 cassettes were introduced via homologous recombination into the *Tacr1*, *Gpr83*, and *Advillin* genes, replacing the first coding ATGs to generate the *Tacr1*^{CreERT2}, *Gpr83*^{CreERT2}, and *Advillin*^{FlpO} mouse lines, respectively. Detailed sequence elements of the targeting vectors are described in Extended Data Fig. 1a. *Robo3* $^{IRES\text{-}CreERT2}$, *Tacr1*^{CreERT2}, *Gpr83*^{CreERT2}, and *Advillin*^{FlpO} heterozygous mice were generated by mating chimeric mice to germline FlpE (*Actb-FlpE*) (JAX#003800) or germline Cre (*EIIa-Cre*) (JAX#003724) mice to remove the neomycin selection cassette. Other published knockin mouse lines used in this study include *Lbx1*^{FlpO} [10], *Rosa26*$^{FSF\text{-}LSL\text{-}tdTomato}$ (Ai65) (JAX#021875), *Rosa26*$^{LSL\text{-}tdTomato}$ (Ai14) (JAX#007908), *Rosa26*$^{LSL\text{-}EYFP}$ (Ai3) (JAX#007903), *Rosa26*$^{LSL\text{-}synaptophysin\text{-}tdTomato}$ (Ai34) (JAX#012570), *Rosa26*$^{FSF\text{-}tdTomato}$ (generated from the cross between Ai65 and *EIIa-Cre* mouse lines; germline excision of LSL), *Rosa26*$^{LSL\text{-}FSF\text{-}ReaChR}$ [31] (JAX#024846), *Rosa26*$^{LSL\text{-}FSF\text{-}TeTx}$ [32], *Rosa26*$^{FSF\text{-}LSL\text{-}Synaptophysin\text{-}GFP}$ [33], *Tac1*$^{IRES2\text{-}Cre}$ (JAX#021877), *Gad2*$^{NLS\text{-}mCherry}$ (JAX#023140), *Advillin*^{Cre} [34], *Ntrk2*^{CreER} [35], *Mrgprb4*^{Cre} [36], and *Mrgprd*^{Cre} [23]. The *Calca-FlpE* BAC transgenic mouse line was generated by introducing a FlpE cassette downstream of the first coding ATG of the *Calca* gene in a bacterial artificial chromosome (RP23-181A2). The *Gpr83-EGFP* BAC transgenic mouse line was imported from the MMRRC (Stock number: 010442-UCD). Other published transgenic mouse lines used in this study include *Cdx2-Cre* (JAX#009352), *Calca-GFP* (MMRRC, Stock number: 011187-UCD) and *Cdx2-NSE-FlpO*[11].

Tamoxifen treatment.

Tamoxifen (T5648, Sigma) was dissolved in 100% ethanol (20 mg/ml), mixed with a 2x volume of sunflower seed oil (S5007, Sigma), vortexed for 20 minutes and vacuum centrifuged for 30 minutes for ethanol evaporation. Tamoxifen in sunflower seed oil (10 mg/ml) was delivered via oral gavage to pregnant female mice for embryonic treatment (3-4 mg at E11.5 for *Robo3*^{CreERT2}) or to mice at weaning ages (P19-P24) for postnatal treatments (1-1.5 mg for *Tacr1*^{CreERT2} and 2-2.5 mg *Gpr83*^{CreERT2}). The number of tamoxifen treatments for *Tacr1*^{CreERT2} and *Gpr83*^{CreERT2} varied depending on reporter mouse lines and Cre-dependent viruses used for experiments; *Rosa26*$^{FSF\text{-}LSL\text{-}tdTomato}$ (Ai65), *Rosa26*$^{LSL\text{-}tdTomato}$ (Ai14), and *Rosa26*$^{LSL\text{-}EYFP}$ (Ai3), *Tau*^{FSFiAP}, one dose; *Rosa26*$^{LSL\text{-}FSF\text{-}ReaChR}$, two doses two days apart; *Rosa26*$^{LSL\text{-}FSF\text{-}TeTx}$, three doses on three

consecutive days; AAV1-FLEX-PLAP, one dose 5-7 days after virus injection; all other Cre-dependent viruses, two to three doses were administered 5-14 days after virus injections.

Surgical procedures.

Spinal cord injections.—Mice (P12-20) were anesthetized via continuous inhalation of isoflurane (1.5 – 2.5 %) using an isofluorane vaporizer (VetEquip) during the surgery. Laminectomies were performed to expose either cervical, thoracic, or lumbar spinal cords, and total 300 – 450 nl of AAV viruses were directly injected into two to three adjacent spots in the spinal cord using pulled glass pipettes (Wiretrol II, Drummond) and a microsyringe pump injector (UMP3, World Precision Instruments). For sparse labeling experiments described in Fig. 4, 150 nl of 1/10 diluted AAV1-hSyn-FlpO-WPRE (1.37E+12gc/ml) was injected into one location in the lumbar spinal cord.

Brain injections and fiberoptic/dual opto-fluid cannula implants.—Mice (6-10 weeks old) were placed on a stereotaxic frame (Kopf Instruments) and anesthetized via continuous inhalation of isoflurane (1.5 – 2.5 %) using an isofluorane vaporizer during the surgery. Burr holes were made on the skull using a dental drill, and 150 – 250 nl of Alexa Fluor-conjugated CTB (ThermoFisher) or 100 – 300 nl of AAV viruses were injected into the target brain regions using pulled glass pipettes (Wiretrol II, Drummond) and a microsyringe pump injector (UMP3, World Precision Instruments). For fiberoptic or dual opto-fluid cannula implants, fiberoptic cannulas (400 μm in diameter, 0.53NA, Doric Lenses) or dual opto-fluid cannulas (DiOFC, Doric Lenses) were bilaterally implanted into the PBN_L and secured using a gel type super glue (Loctite) with an accelerator application followed by dental cement (Metabond, Parkell) application. The coordinates used for stereotaxic injections/implants are as follows; PBN_L (−5.2 – −5.0 mm posterior to bregma, ± 1.4 – 1.6 mm from midline, and −2.8 – −3.0 ventral to dura), MGm/SPFp (−3.05 – −3.15 mm posterior to bregma, −1.70 – −1.75 mm from midline, and −3.0 – −3.2 mm ventral to dura), SCig (−3.35 – −3.50 mm posterior to bregma, −0.75 – −1.25 mm from midline, and −1.35 – −1.45 mm ventral to dura).

Viruses.

The following AAV viruses were used in this study: AAV1-CAG-FLEX-Synaptophysin-GFP-WPRE (1.088E+14gc/ml), AAV1-CAG-FLEX-Synaptophysin-BFP-WPRE (1.5059E +14gc/ml), AAV1-CAG-FLEX-Synaptophysin-tdTomato-WPRE (1.1482E+14gc/ml), AAV2-Retro-CAG-FLEX-tdTomato-WPRE (2.22248E+13gc/ml), AAV2-Retro-EF1α-FlpO-WPRE (2.683E+13gc/ml), AAV1-hSyn-Con/Fon-EYFP-WPRE (1.04E+13gc/ml), and AAV1-hSyn-FlpO-WPRE (1.37E+13gc/ml). pAAV-FLEX-Synaptophysin-GFP expression vector[37] was a gift from Silvia Arber. pAAV-FLEX-Synaptophysin-BFP and pAAV-FLEX-Synaptophysin-tdTomato expression vectors were generated by swapping the GFP sequence with BFP and tdTomato sequences, respectively. pAAV-CAG-FLEX-Synaptophysin-tdTomato-WPRE (Addgene#51503) and pAAV-hSyn-Con/Fon-EYFP-WPRE[38] (Addgene#55650) expression vectors were purchased from Addgene. pAAV-EF1α-FlpO-WPRE and pAAV-hSyn-FlpO-WPRE expression vectors were generated using standard approaches. All the AAV viruses were produced and packaged at the Boston Children's

Hospital Viral Core Facility except for the AAV1-FLEX-PLAP virus, which was a gift from Connie Cepko.

Dual-virus retrograde labeling experiments.—The traditional view of the anterolateral pathway is that most of the spinal PN axons form collateral branches that innervate multiple regions of the brain, including the PBN_L[3]; this is based on double labeling of neurons by retrograde tracers injected into different brain regions. However, one potential caveat of this approach is that some brain targets of the anterolateral pathway, particularly in the hindbrain, including the PBN_L of the pons and brainstem, are located near main bundles of ascending anterolateral pathway axons, potentially complicating interpretation of retrograde labelling experiments because PNs may be labelled by uptake of tracers into fibers of passage as well as axon terminals. To circumvent this concern, we selectively labeled *Tacr1*$^+$ or *Gpr83*$^+$ spinal PNs that innervate rostral brain targets, including the MGm/SPFp of the posterior thalamus and the SCig of the midbrain, by combining lumbar spinal cord injections of AAV1-C_{on}/F_{on}-EYFP viruses[38] and brain injections of AAV2-retro-FlpO viruses[39] into *Tacr1*^{CreERT2} or *Gpr83*^{CreERT2} mice (Extended Data Fig. 3).

AAV1-FLEX-Synaptophysin virus injections into three spinal axial levels.—AAV1-FLEX-Synaptophysin viruses[37] expressing one of three different fluorescent proteins (GFP, BFP, and tdTomato) were injected into three spinal axial levels (lumbar enlargement, mid-thoracic, and cervical enlargement) of either *Tacr1*^{CreERT2} or *GPR83*^{CreERT2} mice to visualize synaptic terminals of SPB neurons representing hindlimbs, thoracic body regions, and forelimbs, respectively (Figure 4g–i, Extended Data Figure 8f).

RNAscope *in situ* hybridization.

Adult mice were euthanized with carbon dioxide. Lumbar spinal cords were dissected and immediately embedded in OCT (1437365, Fisher) and frozen with dry ice-cooled methylbutane. The spinal cord tissues were cyrosectioned (25 μm) using a cryostat (Leica), and transverse sections were collected on glass slides (12–550-15, Fisher). mRNA transcripts were detected using RNAscope Fluorescent Multiplex Assay (Advanced Cell Diagnostics) and RNAscope Fluorescent Multiplex Reagent Kit (Cat. No. 320850). The RNAscope catalog probes were used to detect *Gpr83* (Cat. No. 317431), *Tac1* (Cat. No. 410351) and *tdTomato* (Cat. No. 317041-C2) mRNA molecules.

Immunohistochemistry.

Mice (6 – 8 weeks old) were anesthetized with CO_2 and transcardially perfused with 5-10 mL of modified Ames Media (A1420, Sigma) in 1x PBS, followed by 20–30 mL of 4% paraformaldehyde (PFA) (P6148, sigma or 15714-S, EMS) in 1x PBS at room temperature (RT). Brains and vertebral columns, including spinal cords and dorsal root ganglia, were roughly dissected from perfused mice and post-fixed in 4% PFA at 4°C overnight. Tissues were washed in 1x PBS for over 3 hours, and brains and spinal cords were finely dissected out from the rest of the tissue. Brain and spinal cord tissues were cryoprotected in 30% sucrose in 1x PBS at 4°C for 2 days, embedded in OCT (1437365, Fisher), frozen using dry ice, and kept at −80°C. Brain (coronal sections) and spinal cord (transverse or horizontal

sections) tissues were cyrosectioned (30 - 40 μm) using a cryostat (Leica). Spinal cord sections were collected on glass slides (12-550-15, Fisher) and brain sections were collected on glass slides or in 1x PBS. Sections (on slides for spinal cord sections, on slides or as floating sections for brain sections) were washed 3 times for 5 minutes each with 1x PBS containing 0.1% Triton X-100 (0.1% PBST), incubated with blocking solutions (0.1% PBST containing 5% normal goat serum (S-1000, Vector Labs) or normal donkey serum (005-000-121, Jackson Immuno)) for 1 hour at RT, incubated with primary antibodies diluted in blocking solutions at 4°C overnight, washed 3 times for 10 minutes each with 0.1% PBST, incubated with secondary antibodies diluted in blocking solutions at 4°C overnight, washed again 4 times for 10 minutes each with 0.1% PBST (DAPI solution (D1306, ThermoFisher) was included in the second wash at 1:5000 dilution), and mounted with fluoromount-G (Southern Biotech). IB4 (Alexa 647 conjugated, I32450, ThermoFisher) was diluted at 1:300 and incubated together with secondary antibodies. Primary antibodies used in this study include rabbit anti-DsRed (1:1000, 632496, Clontech), goat anti-mCherry (1:1000, AB0040-200, Acris), chicken anti-GFP (1:1000, GFP-1020, Aves Labs), rabbit anti-GFP (1:1000, A-11122, Life Technologies), mouse anti-NeuN (1:1000, MAB377, Millipore), rabbit anti-tagRFP (for BFP detection, 1:1000, AB233, Evrogen), rabbit anti-TACR1 (1:2000, S8305, Sigma), rabbit anti-PKCγ (1:1000, SC-211, Santa Cruz Biotechnology), mouse anti-c-Fos (1:1000, M-1752-100, Biosensis), rabbit anti-phospho-c-Fos (1:500, #5348, Cell Signaling), and rabbit anti-CGRP (1:1000, 24112, Immunostar). Secondary antibodies included Alexa 488 or 546 conjugated goat anti-rabbit antibodies, Alexa 488 or 546 conjugated goat anti-chicken antibodies, Alexa 488 or 647 conjugated goat anti-mouse antibodies (IgG_1), Alexa 647 conjugated goat anti-guinea pig antibodies, Alexa 488 conjugated donkey anti-chicken antibodies, Alexa 546 conjugated donkey anti-goat antibodies, and Alexa 488 or 647 conjugated donkey anti-rabbit antibodies. All secondary antibodies were purchased from Life Technologies except for Alexa 488 conjugated donkey anti-chicken antibodies, which was purchased from Jackson ImmunoResearch, and used at 1:500 dilution.

Whole-mount alkaline phosphatase (AP) staining.

Mice (6 – 8 weeks old) were euthanized, perfused, fixed, and dissected as described in the immunohistochemistry section. Cortexes and cerebellums were removed, and the remaining tissues, including subcortical regions of the brain and spinal cords, were subjected to heat inactivation of endogenous AP for 2-5 hours at 65-68°C in 1x PBS. The tissues were washed with B1 buffer (0.1 M Tris pH 7.5, 0.15 M NaCl) 3 times for 10 minutes each at RT and then washed with B3 buffer (0.1 M Tris pH 9.5, 0.1 M NaCl, 50 mM $MgCl_2$, 0.1% Tween-20) 3 times for 10 minutes each at RT. The tissues were then incubated with B3 buffer containing NBT(11383213001, Sigma)/BCIP(11383221001, Sigma) (diluted at 3.4 μg/ml each) 0.5 – 1.5 days at RT for AP reactions. The next day, tissues were washed with 1x PBS, fixed with 4% PFA in 1x PBS for over 4 hours at 4°C, serially dehydrated with 50%, 75%, and 100% methanol for 1 hour each, and incubated in fresh 100% methanol overnight. Dehydrated tissues were pinned to a glass dish coated with Sylgard (Sylgard 184 Silicone Elastomer Kit (Dow)), cleared in BABB (BABB: 1 part Benzyl Alcohol (108006, Sigma): 2 parts Benzyl Benzoate (B6630, Sigma)) for 10 - 30 minutes, and then imaged.

Imaging and image analyses.

Fluorescence images.—Z-stack images were taken with a Zeiss LSM 700 confocal microscope using either 10X (Plan-Apochromat 10X/NA 0.45) or 20X (Plan-Apochromat 20X/NA 0.8) objectives. The Tile-scan function was used for imaging large spinal cord and brain sections, and the tile images were stitched using Zeiss Zen microscope software. Fluorescence overlaps (Fig. 1g, h, Extended Data Fig. 1b, c, e, f, 2a–f, j–n, 8b, c), the number of cell bodies of SPB neurons (Extended Data Fig. 7h, i), and the number of Fos^+ neurons (Fig. 2f, g, 5g–j, Extended Data Fig. 4g, h, 6e, f) were analyzed using either Zeiss Zen microscope software (2.3 SP1) or ImageJ (2.0.0-rc-69/1.52p) with Cell Counter plugin mostly by investigators who were blinded to genotype. Average fluorescence intensity of $tdTomato^+$ axons (Fig. 1c–e), fluorescence densities of synaptic terminals in the subnuclei of PBN_L (Fig. 2c, d, Extended Data Fig. 2p, q) and dendritic lengths of SPB neurons (Extended Data Fig. 7h, j, k) were measured using ImageJ. The number of $tdTomato^+$ synaptic terminals of SPB axons associated with GFP^+ cell bodies and neurites (Extended Data Fig. 4a, b) was quantified using custom image analysis modules built with CellProfiler software (3.1.9). The estimation of the percentages of spinal cord *Tacr1*$^+$ and *Gpr83*$^+$ neurons that constitute anterolateral pathway PNs (described in the Extended Data Fig. 6 figure legend) were calculated based on retrograde labeling experiments described in Extended Data Fig. 2e. However, the estimated percentages are lower bounds and almost certainly underestimations because it is unlikely that 100% labeling efficiency was achieved with retrograde tracer injections and because injecting retrograde tracers into all the brain targets of the anterolateral pathway was not feasible.

Bright field images of whole-mount AP stained tissues.—Bright field images of whole-mount AP stained tissues were taken with a Zeiss Axio Zoom.V16 microscope using a 1X objective (PlanNeoFluar Z 1.0x/0.25 FWD 56mm). Sparsely labeled single axons of SPB neurons (Fig. 4d–f) were traced using ImageJ with Simple Neurite Tracer plugin.

Fos induction measurements.

Mice were acclimated in stimulation chambers for two days (20 – 30 minutes each day) before the test day. For high-intensity optogenetic stimulation of SPB axon terminals (Fig. 2f, g, Fig. 5g–j, Extended Data Fig. 4g, h), 6.5 mW blue light (473 nm, 10 Hz, 10 ms pulse width) was delivered through fiberoptic cannulas implanted in the PBN_L four times for 30 seconds each (30 second light-off periods between photostimulation periods). For low-intensity photostimulation (Fig. 5g–j), 0.4 mW blue light (473 nm, 10 Hz, 10 ms pulse width) was delivered either four times for 30 seconds each (30 second light-off periods between photostimulation periods) or 16 times for five seconds each (10 second light-off periods between photostimulation periods). Littermate controls were photostimulated with either of the protocols above. For thermal stimulation (Extended Data Fig. 6e, f), mice were placed either on a 55°C hot plate for 30 seconds or on a 5°C cold plate for 10 minutes. Littermate controls were placed on a plate at room temperature for 10 minutes. 1.5 hours after the delivery of each stimulation, mice were perfused and processed for Fos immunohistochemical analysis.

Ex vivo whole-cell patch-clamp recordings using a skin-spinal cord preparation.

A semi-intact skin-spinal cord preparation was used as previously described[18] with a few modifications. Briefly, mice (6–9 weeks old) were deeply anesthetized with ketamine/xylazine (90 and 10 mg/kg, respectively) and transcardially perfused through the left ventricle with oxygenated (95% O_2 and 5% CO_2) sucrose-based artificial cerebrospinal fluid (ACSF) (in mM; 234 sucrose, 2.5 KCl, 0.5 $CaCl_2$, 10 $MgSO_4$, 1.25 NaH_2PO_4, 26 $NaHCO_3$, 11 Glucose) at room temperature. Immediately after perfusion, the skin was incised along the dorsal midline and the spinal cord was quickly exposed via dorsal laminectomy. The right hindlimb and the spinal cord (~C2 – S6) were dissected, transferred onto Sylgard-coated dissection/recording dish, and submerged in the same sucrose-based ACSF, which was circulated at 50 ml/min for superfusion of the spinal cord. Next, the skin piece innervated by the saphenous nerve and the femoral cutaneous nerve was dissected free of surrounding tissues. The L2 and L3 DRGs were left attached on the spine. Dural and pial membranes were carefully removed and the spinal cord was pinned onto the Sylgard chamber with the right dorsal horn facing upward. After the dissection, the chamber was transferred to the electrophysiology rig, and the skin-spinal cord preparation was perfused with normal ACSF solution (in mM; 117 NaCl, 3.6 KCl, 2.5 $CaCl_2$, 1.2 $MgCl_2$, 1.2 NaH_2PO_4, 25 $NaHCO_3$, 11 glucose) saturated with 95% O_2 and 5% CO_2 at 32°C. The tissues were rinsed with ACSF for at least 30 minutes to wash out sucrose. Thereafter, recordings were performed for up to 6 hours post-dissection. Neurons were visualized using a fixed stage upright microscope (BX51WI, Olympus) equipped with a 40X water immersion objective and a CCD camera (ORCA-ER, Hamamatsu Photonics). A narrow beam infrared LED (L850D-06, Marubeni) was positioned outside the solution meniscus. Either *Tacr1*$^+$ or *Gpr83*$^+$ lamina I SPB neurons were identified by CTB (injected into the PBN_L) and GFP (or tdTomato) double fluorescence. Whole-cell patch-clamp recordings were then performed using a thin-walled single-filamented borosilicate glass pipette pulled with a microelectrode puller (PC-10, Narishige International). The Pipette resistance ranged from 6 to 12 MΩ. Electrodes were filled with an intracellular solution (in mM: 135 K-gluconate, 5 KCl, 0.5 $CaCl_2$, 5 EGTA, 5 HEPES, 5 MgATP, pH 7.2). Signals were acquired using a Axopatch 200B amplifier (Molecular Devices). The data were low-pass filtered at 2 kHz and digitized at 10 kHz with an A/D converter (Digidata 1322A, Molecular Devices) and stored using a data acquisition program (Clampex version 10, Molecular Devices). The liquid junction potential was not corrected. To search for a cell's receptive field, mechanical stimulation with a firm brush or thermal stimulation with hot (50°C) or cold (0°C) saline was applied systematically over the skin. Once a receptive field was located, stimuli were reapplied directly to the receptive field. To record action potential firings following mechanical stimulation, the skin was indented using a range of von Frey filaments (0.16g, 1g, 2g and 4g). To record action potential firings following application of thermal stimuli, saline with various temperatures (0°C, 15°C, 40°C and 54°C) was gently applied to the skin using a 10 ml syringe. To record capsaicin-evoked action potential firings, 0.05% capsaicin (20 μl) dissolved in 100% ethanol was gently applied to the skin. Peak instantaneous firing frequency was used to evaluate the response to each stimulus. The baseline firing rate (average spontaneous firing rate before stimulus) was subtracted from the peak instantaneous firing frequency. Cells that exhibited peak instantaneous firing frequency greater than 2 Hz were counted as responders.

Whole-cell patch-clamp recordings using an acute spinal cord slice preparation.

ReaChR, a red-shifted variant of channelrhodopsin[40], was selectively expressed in distinct primary sensory neuron subtypes using intersectional genetic strategies that combine a sensory neuron subtype specific Flp (or Cre) recombinase mouse line, a pan-sensory neuron-specific *Advillin*^{Cre} line[34] (or a newly generated *Advillin*^{FlpO} line) (Extended Data Fig. 1e, 7a), and the dual recombinase dependent ReaChR mouse line *Rosa26*$^{LSL\text{-}FSF\text{-}ReaChR}$ (Fig. 3h). Whole-cell patch-clamp recordings were then performed on *Gpr83*$^{+}$ and *Tacr1*$^{+}$ SPB neurons labeled with tdTomato by viral delivery of AAV2-Retro-FLEX-tdTomato into the PBN_L of quadruple transgenic mice harboring either the *Tacr1*^{CreERT2} or *Gpr83*^{CreERT2} allele. Acute transverse spinal cord slices were used for whole-cell patch-clamp recordings of retrogradely labeled *Tacr1*$^{+}$ and *Gpr83*$^{+}$ SPB neurons. Specifically, mice (5-7 weeks old) were anesthetized via continuous inhalation of isoflurane (1.5% – 2.5%) while vertebral columns were dissected. Lumbar enlargements were dissected out from vertebral columns in an ice-cold choline solution (in mM: 92 Choline Chloride, 2.5 KCl, 1.2 NaH_2PO_4, 30 $NaHCO_3$, 20 HEPES, 25 Glucose, 5 Sodium Ascorbate, 2 Thiourea, 3 Sodium Pyruvate, 10 $MgSO_4$ $7H_2O$, 0.5 $CaCl_2$ $2H_2O$) and mounted in 0.3% LMP agarose (16520-100, Life Technology). The lumbar spinal cords were sliced in a transverse plane (350 μm) (VT1200S, Leica), and the spinal cord slices were recovered at 34°C for 30 minutes in oxygenated (95% O_2 and 5% CO_2) HEPES holding solution (in mM: 86 NaCl, 2.5 KCl, 1.2 NaH_2PO_4, 35 $NaHCO_3$, 20 HEPES, 25 Glucose, 5 Sodium Ascorbate, 2 Thiourea, 3 Sodium Pyruvate, 1 $MgSO_4$ $7H_2O$, 2 $CaCl_2$ $2H_2O$). After recovery, spinal cord slices were placed at RT for 30 minutes prior to recordings. Spinal cord slices were then superfused with oxygenated (95% O_2 and 5% CO_2) recording ACSF (in mM: 2.5 $CaCl_2$ $2H_2O$, 1.0 NaH_2PO_4 H2O, 119 NaCl, 2.5 KCl, 1.3 $MgSO_4$ $7H_2O$, 26 $NaHCO_3$, 25 Glucose, 1.3 Sodium L-ascorbate) at RT in a recording chamber mounted on a SliceScope Pro 6000 electrophysiology rig (Scientifica). Cells were visualized by fluorescence to identify tdTomato positive cells, followed by infrared differential interference contrast microscopy for patching (ORCA-Flash 4.0, Hamamatsu Photonics; SliceScope Pro 6000, Scientifica). Whole-cell voltage-clamp recordings of retrogradely labeled SPB neurons within superficial lamina were obtained under visual guidance using a 40x objective. The Pipette resistance ranged from 3 to 4 MΩ, and the electrodes were filled with an intracellular solution (in mM: 135 K-gluconate, 5 KCl, 0.5 $CaCl_2$, 5 EGTA, 5 HEPES, 5 MgATP, pH 7.2). Signals were acquired using a Multiclamp 700B amplifier (Molecular Devices). The data were low-pass filtered at 2 kHz and digitized at 10 kHz with an A/D converter (Digidata 1440A, Molecular Devices) and stored using a data acquisition program (Clampex version 10, Molecular Devices). The liquid junction potential was not corrected. Action potential (AP) discharges were recorded in current-clamp mode. For ChR2-assisted circuit mapping, primary afferent synaptic terminals were stimulated with wide-field blue LED illumination through the 40x objective (pE-300, CoolLED, 0.1 ms, 1 ms, and 10 ms pulse width, light intensity = 27 mW). Cell capacitance, current amplitude, latency, and jitter were analyzed using Clampfit (version 10, Molecular Devices). For pharmacology experiments, cells were recorded in a solution containing 1 μM tetrodotoxin (TTX) (1069, Tocris) followed by the addition of 4-aminopyridine (4-AP; 500 μM) (940, Tocris) to the bath.

Tactile and thermal behavioral experiments.

Both male and female mice (2 - 6 months old) of mixed genetic backgrounds were used for behavioral analyses (except for the real-time texture aversion assay in which only male mice were used). All mice (experimental mice and littermate controls) were group housed. Littermates from the same genetic crosses were used as controls for each group to control for variability in mouse strains/genetic backgrounds. Experiments were performed and analyzed by investigators who were blinded to genotype.

von Frey test.—Mice were placed in clear plastic chambers on an elevated wire mesh and the plantar surface of the hindpaw was stimulated with a set of calibrated von Frey filaments (North Coast Medical) 10 times each (0.008 - 4 g). The number of paw withdrawal responses was scored for each von Frey filament.

Hot/cold plate.—Mice were placed on a 55°C hot plate or a 5°C cold plate (IITC) and their behaviors were recorded using a camera (Hero 4, GoPro). Cut-off times were 20 seconds and 3 minutes for 55°C hot plate and 5°C cold plate, respectively. The number of paw-licking episodes (hindpaw licking for hot plate and forepaw licking for cold plate) were manually scored by analyzing video recordings.

Real-time texture aversion.—Male mice were habituated in test chambers (black acrylic, 12 inches x 11.8 inches x 6 inches, 0.25 inch-thickness) for 2 days (10 - 20 minutes each day) prior to the test day. On the test day, mice were first placed in test chambers with a fresh sheet of dusty pink construction paper (338293, Office Depot) on the floor and their baseline preference behaviors were recorded for 10 minutes using a digital USB 2.0 CMOS video camera (60516, Stoelting) mounted directly above the test chambers. Mice were then transferred to the test chambers with sandpapers of two different textures (extra fine grit SP400 (smooth) and coarse grit SP150 (rough), McMaster-Carr) on the either side of the floor and their behaviors were recorded for 10 minutes. The mouse centroid was tracked, and the percentage of time spent on each side of the test chamber was analyzed using a custom program written in Bonsai software (2.3.1)[41].

Optogenetic behavioral experiments.

The same criteria were used for mouse handling as described above. Prior to experiments, fiberoptic cannulas implanted into the PBN_L were attached through zirconia sleeves (Doric Lenses) to branching fiberoptic patchcords (Doric Lenses) connected to a blue LED (Doric Lenses) and a programmable LED driver (Doric Lenses). Optogenetic stimulation was controlled by the combination of custom programs written in Bonsai software and Doric Neuroscience Studio (4.1.5.2) through an Arduino circuit board (Uno, Arduino) and custom sketches written in Arduino software (1.8.7). Approximately the initial half of the experiments were performed and analyzed by investigators who were not blinded to genotype, and the remainder of the experiments were repeated by investigators who were blinded to genotype.

Locomotion and grooming analyses.—Mice were habituated in test chambers (Clear acrylic, 8.5 inches x 4.5 inches x 5.5 inches, 0.25 inch-thickness) for 2 days (20 minutes

each day) prior to the test day. On the test day, mice were placed in test chambers and photostimulation was delivered as described in the figure legends. Locomotor and grooming behaviors were recorded (30 frames/second) with two separate digital USB 2.0 CMOS video cameras mounted directly above and in front of the test chambers. The mouse centroid was tracked, and speed and velocity of mouse locomotion were analyzed at 2 Hz with video files filmed by the camera mounted above of the test chambers using a custom program written in Bonsai software. Mouse grooming and jumping behaviors were analyzed manually using video files filmed by the camera mounted in front of the test chambers by investigators who were blinded to genotype.

NBQX infusion.—300 nl of either saline or the selective AMPA receptor antagonist NBQX (10 mM dissolved in saline, 1044, Tocris) was bilaterally infused into the PBN_L through fluid injectors (Doric Lenses) inserted into the dual opto-fluid cannulas implanted into the PBN_L (infusion rate was 100 nl / min). After the infusion, fluid injectors were swapped with optical injectors (Doric Lenses) for photostimulation. Locomotor behavior was monitored 0.5 – 1.5 hours after the infusion.

Pupilometry.—Mice were implanted with custom-cut headplates, which were then secured by dental cement (Metabond, Parkell) application. After 3-5 days of recovery, mice were head-fixed and acclimated on the custom-built behavioral apparatus for 2 days (20 - 30 minutes each day) prior to the test day. On the test day, mice were head-fixed and acclimated on the behavioral apparatus for 10 - 20 minutes, and a photostimulation was delivered as described in the figure legends. Pupillary reactions were recorded (30 frames/second) using a digital USB 2.0 CMOS video cameras mounted close to one eye. An infrared illuminator was used to obtain high contrast images of the pupil. The pupil diameter was tracked at 10 Hz using a custom program written in Bonsai software, and peak amplitude and area under the curve (AUC) were analyzed using GraphPad Prism (Version 8, GraphPad Software). Relative change in pupil diameter (ΔD/D) was calculated as follows.

$$\frac{\Delta \mathrm{D}\ (pupil\ diameter\ -\ average\ baseline\ pupil\ diameter)}{\mathrm{D}\ (average\ baseline\ pupil\ diameter)}$$

The average baseline pupil diameter was the average of pupil diameter during the one-minute baseline period before the beginning of the first optogenetic stimulation. The long abrupt downward lines in the raw traces of pupil diameter were used as a measure of the number of blinks/squints.

Real-time place preference.—Mice were habituated in test chambers (black acrylic, 12 inches x 11.8 inches x 6 inches, 0.25 inch-thickness) for 2 days (20 minutes each day) prior to the test day. On the test day, mice were placed in test chambers and their preference behaviors during pre-stimulation, stimulation, and post-stimulation sessions (10 minutes each session) were recorded using a digital USB 2.0 CMOS video camera mounted directly above the test chambers. The mouse centroid was tracked real-time using a custom program written in Bonsai software, and photostimulation (10 Hz, 10 ms pulse width) was constantly delivered through Doric Neuroscience Studio and Arduino coupled to the Bonsai program

while mice stayed on one side - "stimulated" side - of the chambers (counterbalanced between the two sides).

Lever-pressing assay.—Two levers (ENV-110M, Med Associates) were placed side by side on one side of the test chambers (black acrylic, 10 inches x 8 inches x 8 inches, 0.25 inch-thickness). The original snap action switches inside of the levers were swapped with ones that have lower operating force threshold (480-3021-ND, Digi-Key). The levers were calibrated using von Frey filaments to operate following 4 - 6 g force application. Mice were habituated in test chambers for 2 days (1 hour each day) prior to the test day, and the number of lever presses during the 1-hour session on the third day was used as baseline. During the subsequent eight days ("light on" sessions, 1-hour session each day), mice received an optogenetic stimulation (5 seconds, 10 Hz) when they pressed the active lever, but not the inactive lever (counterbalanced between left and right sides). The active lever was coupled to optogenetic stimulation through Doric Neuroscience Studio and Arduino under control of a custom program written in Bonsai software. The following 5 days ("light off" sessions, 1-hour session each day), optogenetic stimulation was uncoupled from lever-pressing. The number of lever presses was recorded in real-time using custom programs written in Arduino and Bonsai software.

Statistical analysis.

Statistical analyses were performed using GraphPad Prism (Version 8, GraphPad Software). The number of mice used and statistical analyses, including *post hoc* multiple comparisons tests, used for individual experiments are indicated in the figure legends. The following symbols were used in the figure legends for *p*-values: ns, not significant; *, $p < 0.05$; **, $p < 0.01$; ***, $p < 0.001$. The exact *p*-values can be found in the supplementary table 1.

Reporting summary.

Further information on experimental design is available in the Nature Research Reporting Summary linked to this paper.

Data availability.

The data generated in this study are available from the corresponding author upon reasonable request.

Code availability.

The custom codes used in the study are available at GitHub (https://github.com/SebastianChoi/Choi-et-al-Nature2020) or upon request.

Extended Data

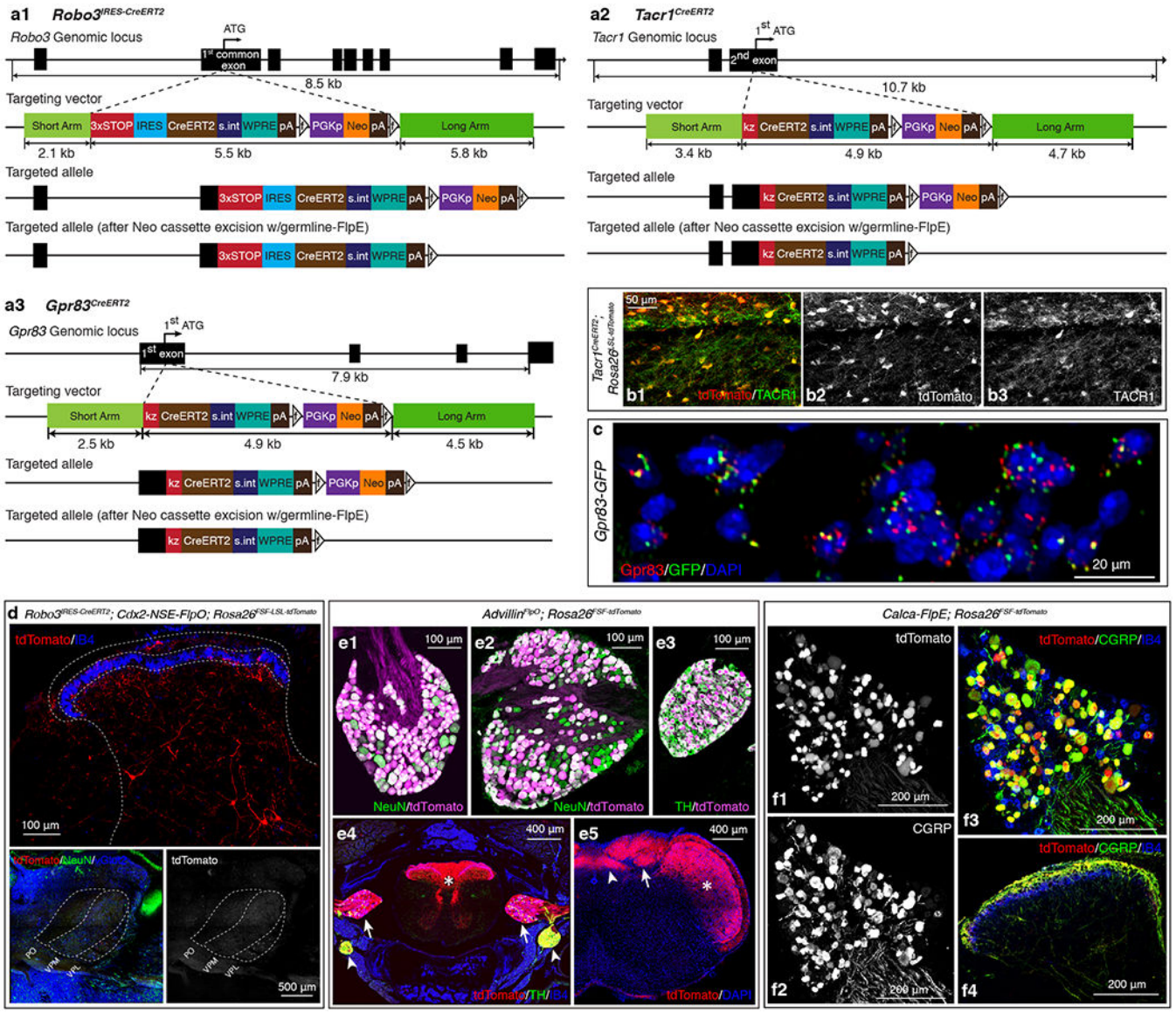

Extended Data Figure 1. Generation of CreERT2 mouse lines for genetic labeling of anterolateral pathway neurons and Flp mouse lines for labeling primary sensory neurons.

a1-a3, Gene targeting strategies used to generate the *Robo3*$^{IRES\text{-}CreERT2}$ (a1), *Tacr1*^{CreERT2} (a2), and *Gpr83*^{CreERT2} (a3) mouse lines. **a1**, A 3X-STOP-IRES-CreERT2 cassette was introduced via homologous recombination into the first common coding exon that is shared by different splice variants of the *Robo3* gene. **a2**, A CreERT2 cassette was introduced via homologous recombination into the *Tacr1* gene, replacing the first coding ATG. **a3**, A CreERT2 cassette was introduced via homologous recombination into the *Gpr83* gene, replacing the first coding ATG. IRES, internal ribosome entry site; s.int, synthetic intron; WPRE, Woodchuck Hepatitis Virus (WHP) Posttranscriptional Regulatory Element; pA, poly A; f, FRT site; kz, kozak sequence. **b1-b3**, A horizontal section of the lumbar spinal cord. 93.7 ± 2.6 % of tdTomato^{+} neurons were *Tacr1*$^{+}$, while 96.6 ± 2.4 % of *Tacr1*$^{+}$ neurons

were tdTomato$^+$. n = 3 mice. **c**, A transverse section of a *Gpr83-GFP* mouse. Green and red dots represent GFP and *Gpr83* mRNA molecules, respectively, detected with gene-specific RNAscope probes. 96.0 ± 1.2% of GFP$^+$ cells were *Gpr83*$^+$, while 84.5 ± 5.0% of *Gpr83*$^+$ cells were GFP$^+$. n = 2 mice. **d**, Distribution of tdTomato-expressing *Robo3*$^+$ neurons in the spinal cord dorsal horn (top) and their thalamic projections terminating in the VPL (bottom). n = 2 mice. **e1-5**, Characterization of the *Advillin*^{FlpO} mouse line. n = 4 mice. **e1-e3**, The *Advillin*^{FlpO} mouse line labels the majority of DRG neurons (99.0 ± 0.1% of NeuN$^+$ neurons are tdTomato$^+$) (e1), nodose ganglia neurons (80.8 ± 5.1% of NeuN$^+$ neurons are tdTomato$^+$) (e2), and sympathetic ganglia neurons (98.6 ± 0.3% of TH$^+$ neurons are tdTomato$^+$) (e3). **e4**, A transverse section of the vertebral column. tdTomato$^+$ Advillin-expressing neurons and their axons are visualized in the spinal cord (asterisk), DRGs (arrows), and sympathetic ganglia (arrowheads). **e5**, A coronal section of the brainstem. tdTomato$^+$ axons of Advillin-expressing neurons innervate the nucleus of the solitary tract (arrowhead), the dorsal column nuclei (arrow), and the trigeminal nucleus (asterisk). **f1-4**, Characterization of the *Calca-FlpE* mouse line. n = 2 mice. A cross section of the lumbar DRG (f1-f3) and a transverse section of the lumbar spinal cord (f4). **f1-3**, 91.9 ± 1.5 % of tdTomato$^+$ neurons were CGRP$^+$, while 92.3 ± 1.5 % of CGRP$^+$ neurons were tdTomato$^+$. **f4**, tdTomato-expressing axons of CGRP$^+$ DRG neurons are CGRP immunoreactive in the spinal cord dorsal horn.

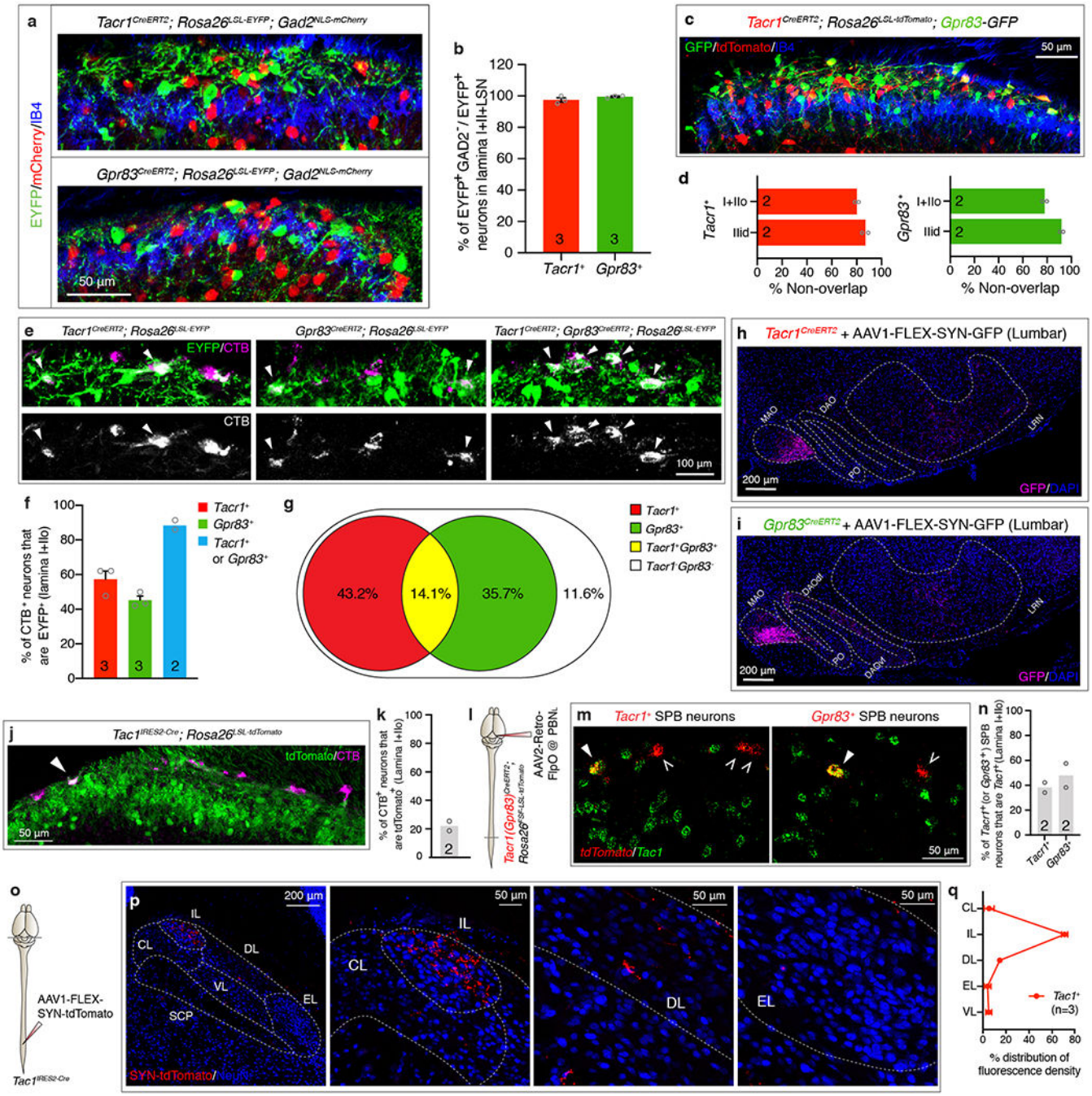

Extended Data Figure 2. Comparative analysis of the *Gpr83*$^+$, *Tacr1*$^+$, and *Tac1*$^+$ SPB populations.

a, Distribution of EYFP-expressing *Tacr1*$^+$ (top) or *Gpr83*$^+$ (bottom) spinal neurons and mCherry-expressing *Gad2*$^+$ neurons in the superficial lamina of the spinal cord dorsal horn. **b**, Quantification of % of *Gad2*-negative neurons in EYFP$^+$ neurons. 97.5 ± 1.4 % of *Tacr1*$^+$ neurons and 99.5 ± 0.5 % of *Gpr83*$^+$ neurons were *Gad2*-negative. **c**, Distribution of tdTomato-expressing *Tacr1*$^+$ neurons and GFP-expressing *Gpr83*$^+$ neurons in the spinal cord dorsal horn. **d**, Quantification of co-expression of tdTomato and GFP. 80.2 ± 1.5% and 87.0

± 2.5% of tdTomato-expressing *Tacr1*$^{+}$ neurons are not positive for GFP expression in lamina I+IIo and lamina IIid, respectively. Conversely, 78.0 ± 1.8% and 92.0 ± 1.4% of GFP-expressing *Gpr83*$^{+}$ neurons are not positive for tdTomato expression in lamina I+IIo and lamina IIid, respectively. **e,** Distribution of EYFP-expressing *Tacr1*$^{+}$ neurons, *Gpr83*$^{+}$ neurons, or both in the superficial lamina of the spinal cord dorsal horn. The SPB neurons were retrogradely labeled with CTB injected into the PBN_L. Arrowheads, CTB and EYFP double-positive neurons. **f**, Quantification for % of *Tacr1*$^{+}$ SPB neurons, *Gpr83*$^{+}$ SPB neurons, and either *Tacr1*$^{+}$ or *Gpr83*$^{+}$ SPB neurons. **g**, % of *Tacr1*$^{+}$, *Gpr83*$^{+}$, *Tacr1*$^{+}$ *Gpr83*$^{+}$, and Tacr1^{-} Gpr83^{-} SPB neurons calculated from experiments in e, f. **h**, **i**, Coronal sections of the ventral brain stem of *Tacr1*^{CreERT2} (f) or *Gpr83*^{CreERT2} (h) mice whose lumbar spinal cords were injected with AAV1-FLEX-Synaptophysin-GFP viruses. MAO, medial accessory olivary nucleus; DAOdf, dorsal accessory olivary nucleus dorsal fold; DAOvf, dorsal accessory olivary nucleus ventral fold; PO, primary olivary nucleus. **j**, Distribution of tdTomato-expressing *Tac1*$^{+}$ neurons in the superficial lamina of the spinal cord dorsal horn. The SPB neurons were retrogradely labeled with CTB injected into the PBN_L. Arrowhead, CTB and tdTomato double-positive neuron. **k**, Quantification of % of *Tac1*$^{+}$ SPB neurons. **l**, Schematic of injections of AAV2-retro-FlpO viruses into the PBN_L. **m**, Distribution of tdTomato-expressing *Tacr1*$^{+}$ (left) or *Gpr83*$^{+}$ (right) SPB neurons and *Tac1*-expressing neurons in the spinal cord dorsal horn. tdTomato (red) and *Tac1* (green) mRNA molecules were detected with gene-specific RNAscope probes. Filled arrowheads, double-positive neurons; empty arrowheads, tdTomato^{+} SPB neurons that do not express *Tac1*. **n**, Quantification of co-expression of tdTomato and *Tac1* in lamina I+IIo. **o**, Schematic of lumbar injections of an AAV1-FLEX-Synaptophysin-tdTomato virus. **p**, Distribution of tdTomato-positive synaptic terminals of *Tac*1^{+} SPB neurons in the PBN_L. **q**, Quantification of distribution of tdTomato-positive synaptic terminals of *Tac1*$^{+}$ SPB neurons in the PBN_L. n = number of mice (indicated in the graph). Error bars, s.e.m.

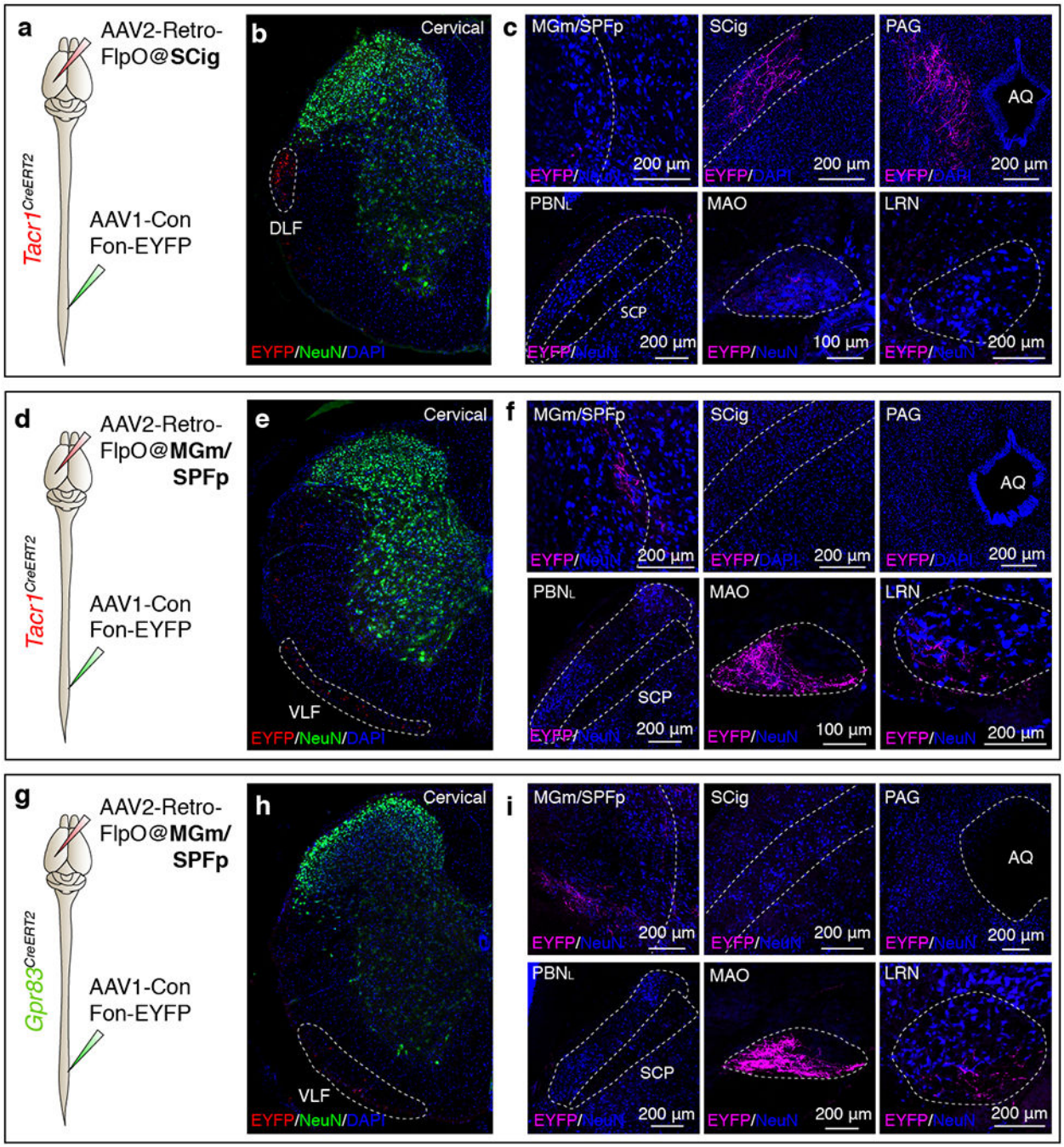

Extended Data Figure 3. *Tacr1*$^{+}$ and *Gpr83*$^{+}$ spinal PNs that innervate the posterior thalamus, midbrain, or the pons are distinct populations.

a, **d**, **g**, Schematics of lumbar spinal cord injections of AAV1-C_{on}/F_{on}-EYFP viruses and brain injections of AAV2-retro-FlpO viruses into the SCig of *Tacr1*^{CreERT2} mice (a) (n = 3 mice), the MGm/SPFp of *Tacr1*^{CreERT2} (d) (n = 2 mice) or *Gpr83*^{CreERT2} mice (g) (n = 3 mice). **b**, **e**, **h**, Transverse sections of cervical spinal cords of *Tacr1*^{CreERT2} (b, e) or *Gpr83*^{CreERT2} mice (h). White dotted lines, tdTomato-expressing axons traveling through spinal cord white matter. DLF, dorsal lateral funiculus; VLF, ventral lateral funiculus. **c**, **f**, **i**,

Coronal sections of target brain regions of *Tacr1*$^+$ (c, f) or *Gpr83*$^+$ (i) spinal PNs. AQ, cerebral aqueduct.

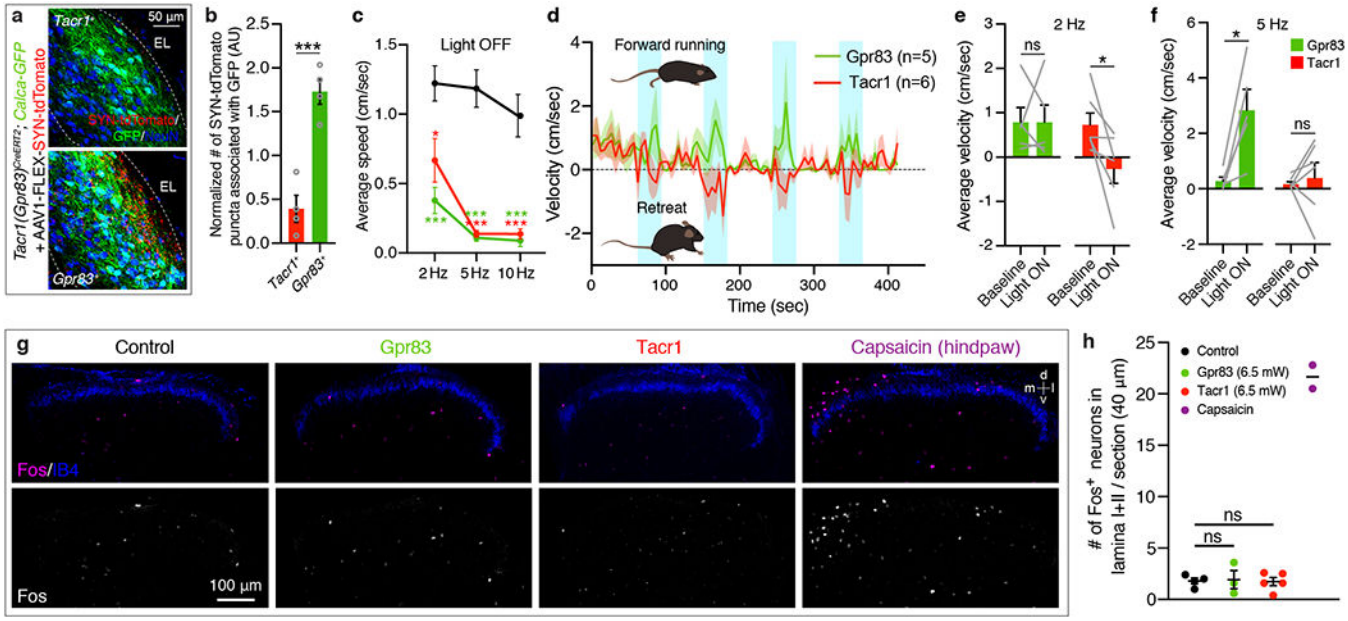

Extended Data Figure 4. Strong axon terminal stimulation of *Tacr1*$^+$ and *Gpr83*$^+$ SPB neurons produces distinct locomotor behaviors.

a, Association of synaptic terminals of *Tacr*1$^+$ and *Gpr83*$^+$ SPB neurons with *Calca-GFP*-expressing cell bodies and neurites in the PBN_{EL}. **b**, Quantification of the number of synaptophysin-tdTomato puncta associated with GFP$^+$ cell bodies and neurites. The numbers were normalized with the total GFP$^+$ area (to normalize for the variability of total GFP$^+$ area) and the total number of synaptophysin-tdTomato puncta within the entire PBN_L (to normalize for the variability of virus injections). AU, arbitrary unit. Two-tailed *t*-test; n = 4 mice each for *Tacr1*$^+$ and *Gpr83*$^+$ SPB neurons. **c**, Quantification of average speed during light-off periods following light-on periods (473 nm, 6.5 mW, 10 ms pulse width). One-way ANOVA (Dunnett's multiple comparisons test); $F_{[2, 16]} = 10.60$ (2 Hz), $F_{[2, 16]} = 40.12$ (5 Hz), $F_{[2, 16]} = 20.48$ (10 Hz). **d**, Average velocity of mice over time (6.5 mW, 2 Hz, 10 ms pulse width). Positive values indicate forward movement whereas negative values indicate backward movement. Shaded areas, s.e.m. **e**, **f**, Quantification of average velocity during light-on periods with 2 Hz (e) and 5 Hz (f) photostimulation. Note that mice receiving *Tacr1*$^+$ SPB neuron terminal stimulation exhibited net negative velocity during the 2 Hz photostimulation and lack a velocity increase despite the dramatic increase in speed during 5 Hz photostimulation. Two-tailed *t*-test; n = 6, 5 mice for Tacr1, Gpr83, respectively. **g**, Distribution of Fos$^+$ neurons in the spinal cord dorsal horn following either photostimulation of axon terminals of SPB neurons (*Tacr1*$^+$ or *Gpr83*$^+$) or a capsaicin (0.1%) injection into a hindpaw. Photostimulation of axon terminals of SPB neurons did not induce significant Fos expression in the spinal cord, whereas a hindpaw injection of capsaicin induced strong Fos expression in the medial region of the superficial lamina of the spinal cord dorsal horn. d, dorsal; v, ventral, m, medial; l, lateral. n = 4, 3, 5, 2 mice for control, Gpr83, Tacr1, Capsaicin, respectively. **h**, Quantification of the number of Fos$^+$ neurons in lamina I and II.

The number of Fos$^+$ cells was quantified in the medial 200 μm of the spinal cord dorsal horn. One-way ANOVA (Tukey's multiple comparisons test). Error bars, s.e.m.

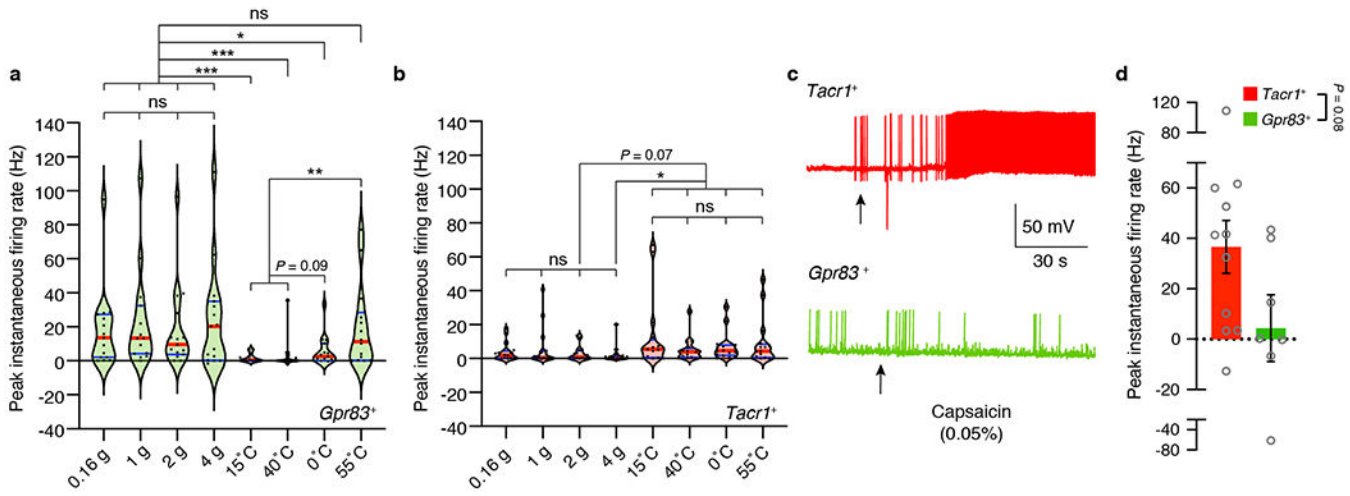

Extended Data Figure 5. Physiological response properties of *Tacr1*$^+$ and *Gpr83*$^+$ SPB neurons.

a, **b**, Summary violin plots of peak instantaneous firing rates of *Gpr83*$^+$ (a) and *Tacr1*$^+$ (b) SPB neurons in response to von Frey indentations and thermal stimuli. Red lines indicate median, while blue lines indicate quartiles. Friedman test (Dunn's multiple comparison test). n = 16, 15 neurons for *Tacr1*$^+$, *Gpr83*$^+$, respectively. **c**, Representative traces of action potential firing evoked by topical capsaicin (0.05%) treatment. Arrows, time when capsaicin was applied to the skin. **d**, Quantification of peak instantaneous firing rates upon capsaicin application. Mann-Whitney test (two-tailed); *p* value is indicated; n = 11, 7 neurons for *Tacr1*$^+$, *Gpr83*$^+$, respectively; error bars, s.e.m.

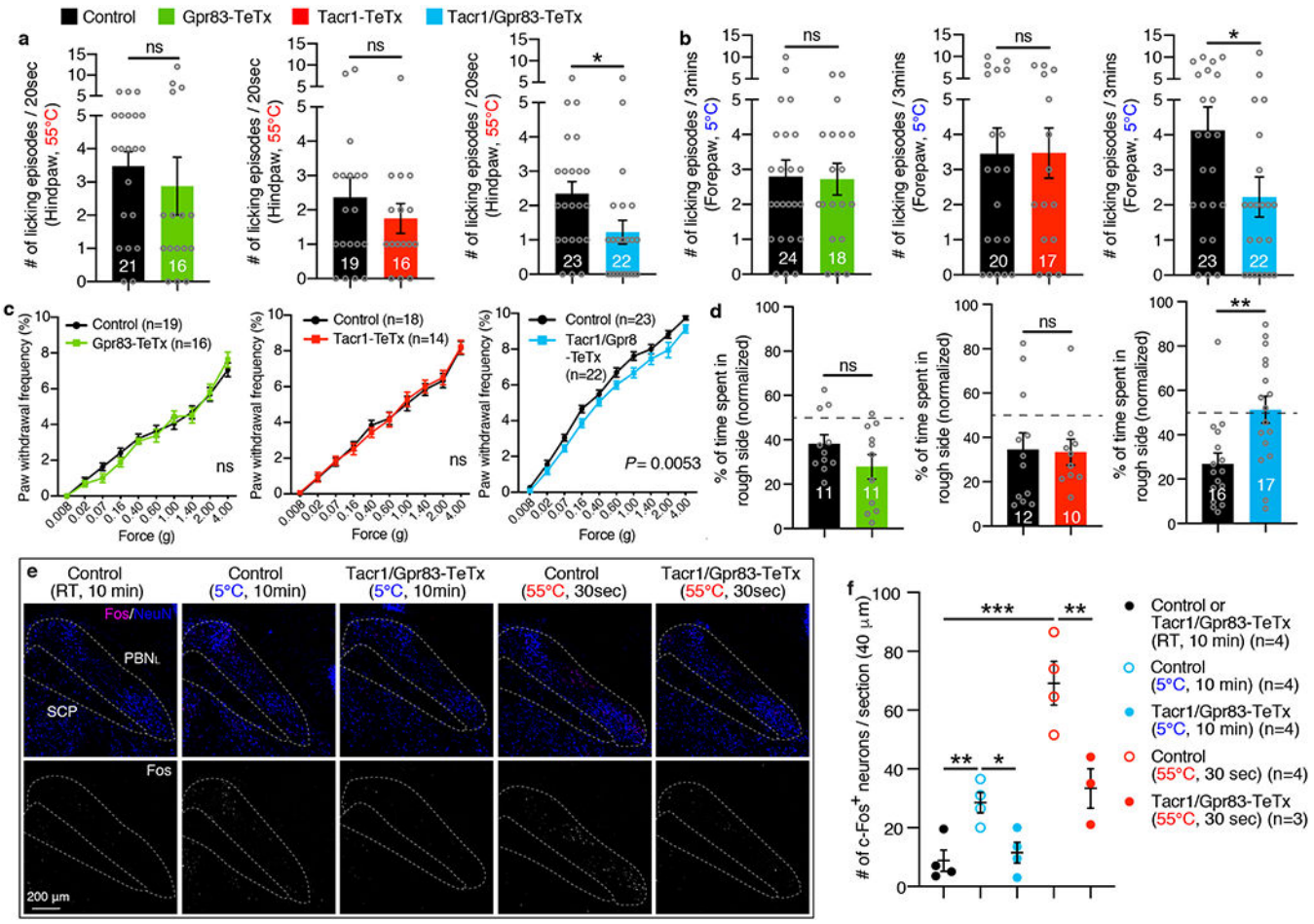

Extended Data Figure 6. Simultaneous inhibition of the synaptic outputs of both *Tacr1*$^+$ and *Gpr83*$^+$ SPB neurons attenuates nocifensive behaviors in response to noxious cutaneous stimuli.

a, Hindpaw-licking was scored while *Tacr1*^{CreERT2}; *Lbx1*^{FlpO}; *Rosa26*$^{LSL\text{-}FSF\text{-}TeTx}$ mice, *Gpr83*^{CreERT2}; *Lbx1*^{FlpO}; *Rosa26*$^{LSL\text{-}FSF\text{-}TeTx}$ mice, or *Tacr1*^{CreERT2}; *Gpr83*^{CreERT2}; *Lbx1*^{FlpO}; *Rosa26*$^{LSL\text{-}FSF\text{-}TeTx}$ mice were placed on the 55°C hot plate (cut-off time, 20 seconds). These intersectional strategies target the entire *Tacr1*$^+$ and *Gpr83*$^+$ spinal populations, of which 34.2% (20.5% PBN_L-projecting, 6.6% PAG-projecting, and 7.1% MGm/SPFp-projecting PNs are combined) and 30.9% (14.0% PBN_L-projecting, 4.6% PAG-projecting, and 12.3% MGm/SPFp-projecting PNs are combined) are *Tacr1*$^+$ and *Gpr83*$^+$ PNs (laminaI/IIo and the LSN are combined), respectively (a detailed description of the quantification is in the methods). Two-tailed *t*-test. **b**, Forepaw-licking was scored while mice were placed on the 5°C cold plate (cut-off time, 3 minutes). Two-tailed *t*-test. **c**, Paw withdrawal frequency following hindpaw skin indentation using von Frey filaments was scored. Two-way ANOVA; *p* value is indicated; $F_{[1, 43]} = 8.65$ for Tacr1/Gpr83-TeTx. **d**, Real-time texture aversion assay (150 grit sand paper vs 400 grit sand paper). % of time spent in rough side of sand paper (150 grit) was measured (normalized to baseline preference). Two-tailed *t*-test. **e, f,** The suppression of neurotransmission in the quadruple transgenic mice was confirmed by reduced Fos induction in the PBN_L following exposure of mice to noxious thermal stimuli. **e**, Distribution of Fos$^+$ neurons in the PBN_L following

thermal stimulation. **f**, Quantification of the number of Fos$^+$ neurons in the PBN$_L$. One-way ANOVA (Tukey's multiple comparisons test); $F_{[2, 9]} = 8.97$ (5°C), $F_{[2, 8]} = 27.09$ (55°C). n = number of mice (indicated in the graphs). Error bars, s.e.m.

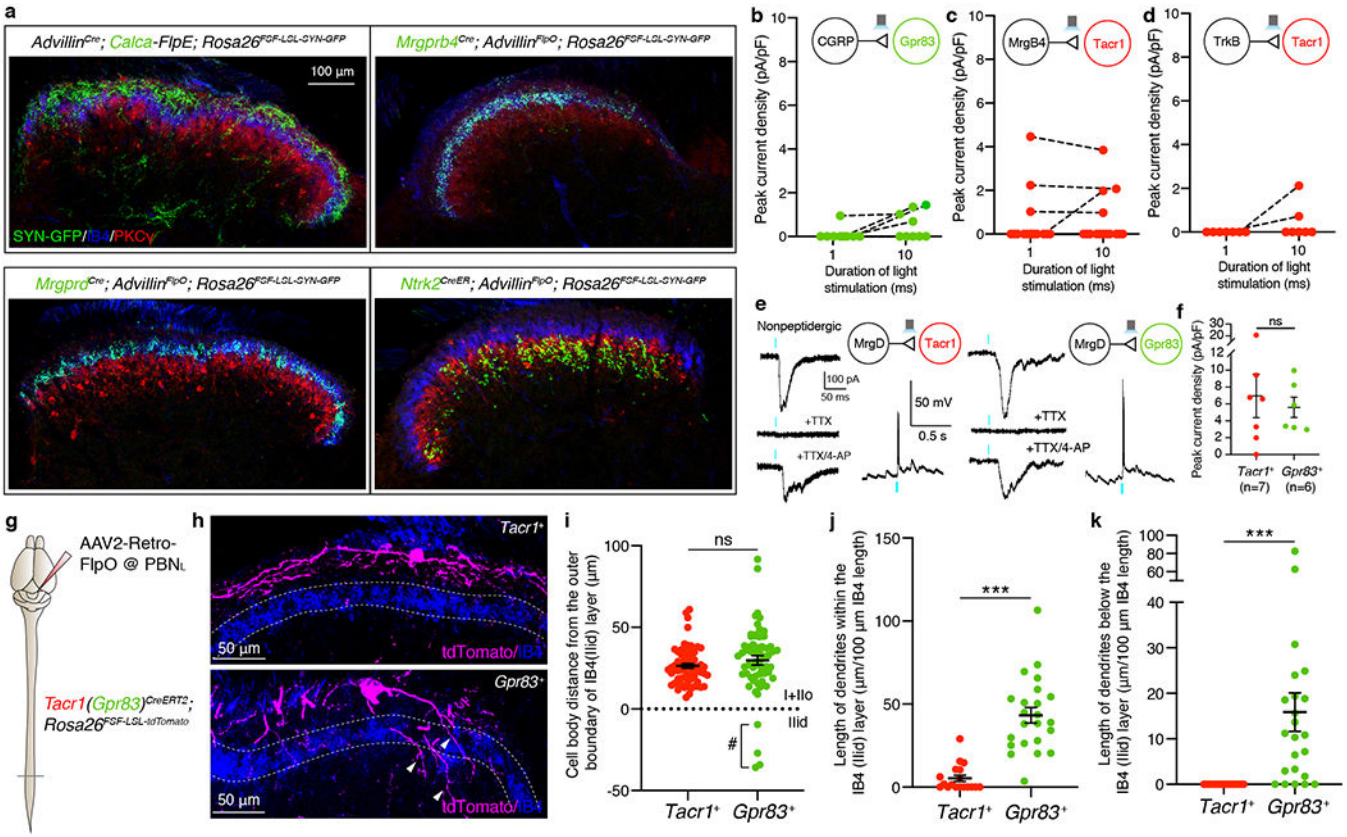

Extended Data Figure 7. *Gpr83*$^+$ and *Tacr1*$^+$ SPB neurons receive strong synaptic inputs from *Mrgprd*$^+$ polymodal non-peptidergic sensory neurons and weak, sparse, and polysynaptic inputs from distinct primary sensory neurons, and exhibit distinct dendritic morphologies.

a, Distribution of CGRP$^+$, *Mrgprb4*$^+$, *Mrgprd*$^+$, and *Ntrk2*$^+$ primary afferent synaptic terminals in the spinal cord dorsal horn. The *Rosa26*$^{FSF\text{-}LSL\text{-}SYN\text{-}GFP}$ reporter mouse line[33] was used in combination with sensory neuron Cre/FlpE mouse lines and *Advillin*^{FlpO}/*Advillin*^{Cre} mouse lines. Note that CGRP$^+$, *Mrgprb4*$^+$, *Mrgprd*$^+$, and *Ntrk2*$^+$ primary afferent synaptic terminals mainly innervate lamina I+IIo, IIid, IIid, and IIiv+III, respectively. **b-d**, Quantifications of peak current density in *Tacr1*$^+$ (c, d) and *Gpr83*$^+$ (b) SPB neurons elicited by long light pulse-stimulation (1 ms and 10 ms) of CGRP$^+$ (b), *Mrgprb4*$^+$ (c), and *Ntrk2*$^+$ (d) primary afferent terminals. The same neurons, stimulated with different durations of light stimulation, are connected by dotted lines. Note that only a small fraction of *Gpr83*$^+$ SPB neurons exhibited long-latency (21.68 ± 2.66 ms), high-jitter (2.97 ± 0.85 ms) polysynaptic EPSCs with 10 ms-long photostimulation of CGRP$^+$ afferent terminals and, conversely, only a small fraction of *Tacr1*$^+$ SPB neurons exhibited long-latency (14.29 ± 3.49 ms), high-jitter (4.31 ± 2.31 ms) polysynaptic EPSCs with 10 ms-long photostimulation of *Mrgprb4*$^+$ afferent terminals. 2 out of 7 *Tacr1*$^+$ SPB neurons exhibited long-latency (11.89 ± 4.18 ms), but relatively low-jitter (0.57 ± 0.21 ms) synaptic EPSCs following 10 ms-long photostimulation of *Ntrk2*$^+$ afferent terminals. **e**, Representative traces

of light-activated currents (left) and AP firing (right) upon photostimulation of *Mrgprd*$^+$ primary afferent terminals. Turquoise bars, 0.1 ms (EPSCs) and 1 ms (APs) LED (473 nm) stimulations. **f**, Quantifications of peak current density. Mann-Whitney test (two-tailed); n = number of neurons. **g**, Schematic of injections of AAV2-retro-FlpO viruses into the PBN_L. **h**, Distribution of tdTomato-expressing dendrites of *Tacr1*$^+$ (top) and *Gpr83*$^+$ (bottom) SPB neurons. Lamina IIid is labeled using IB4 binding. Arrowheads, *Gpr83*$^+$ dendrites that are extended into deeper lamina of the spinal cord dorsal horn. **i**, Quantification of distance between the cell bodies and the outer boundary of IB4$^+$ lamina IIid (dotted line). #, note that a small number of *Gpr83*$^+$ SPB neurons have their cell bodies located within lamina IIid. n = 65, 60 neurons for *Tacr1*$^+$, *Gpr83*$^+$, respectively. **j**, **k**, Quantifications of total length of dendrites in a spinal cord section image within (j) or below (k) IB4$^+$ lamina IIid (normalized to the total length of the IB4$^+$ lamina IIid in the same spinal cord section image). Two-tailed *t*-test; n = 18, 23 sections (40 μm) for *Tacr1*$^+$, *Gpr83*$^+$, respectively. Error bars, s.e.m.

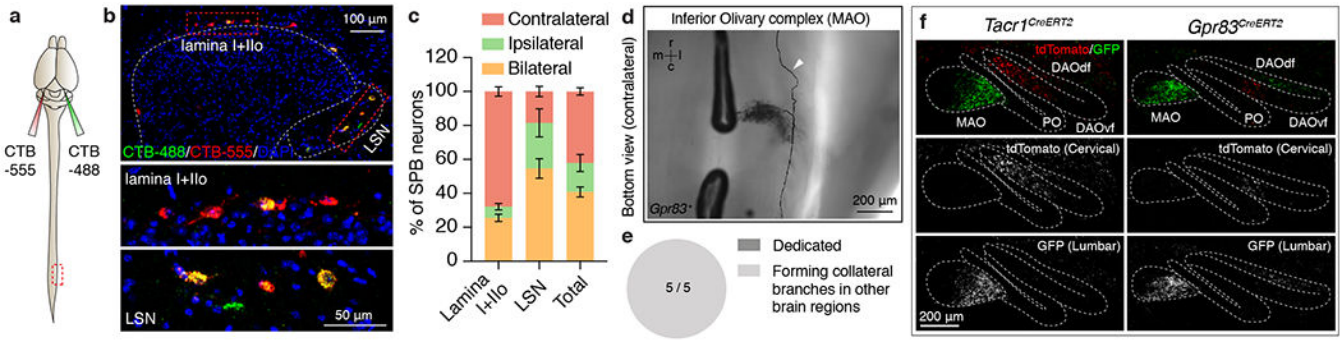

Extended Data Figure 8. Anatomical analyses of axonal projections of anterolateral pathway PNs innervating the PBN_L and the inferior olivary complex.

a, Schematic of dual-CTB injections into the PBN_L. **b**, Distribution of CTB-labeled neurons in the spinal cord lamina I+IIo and the LSN. **c**, Quantification of % of SPB neurons that innervate the PBN_L contralaterally, ipsilaterally, or bilaterally. n = 3 mice. Error bars, s.e.m. **d**, Bottom view of a single axon trace of sparsely labeled *Gpr83*$^+$ spinal PN that innervate the inferior olivary complex. Arrowhead, an axon branch traveling up to the rostral brain. r, rostral; c, caudal, m, medial; l, lateral. **e**, Quantification of the number of inferior olivary complex-projecting spinal PNs that exhibit dedicated vs. collateral-forming axons. **f**, Synaptic terminals of *Tacr1*$^+$ (h) or *Gpr83*$^+$ (i) PNs representing hindlimb regions (GFP) and forelimb regions (tdTomato), are segregated in the inferior olivary complex. n = 3 mice each for *Tacr1*$^+$ and *Gpr83*$^+$ PNs.

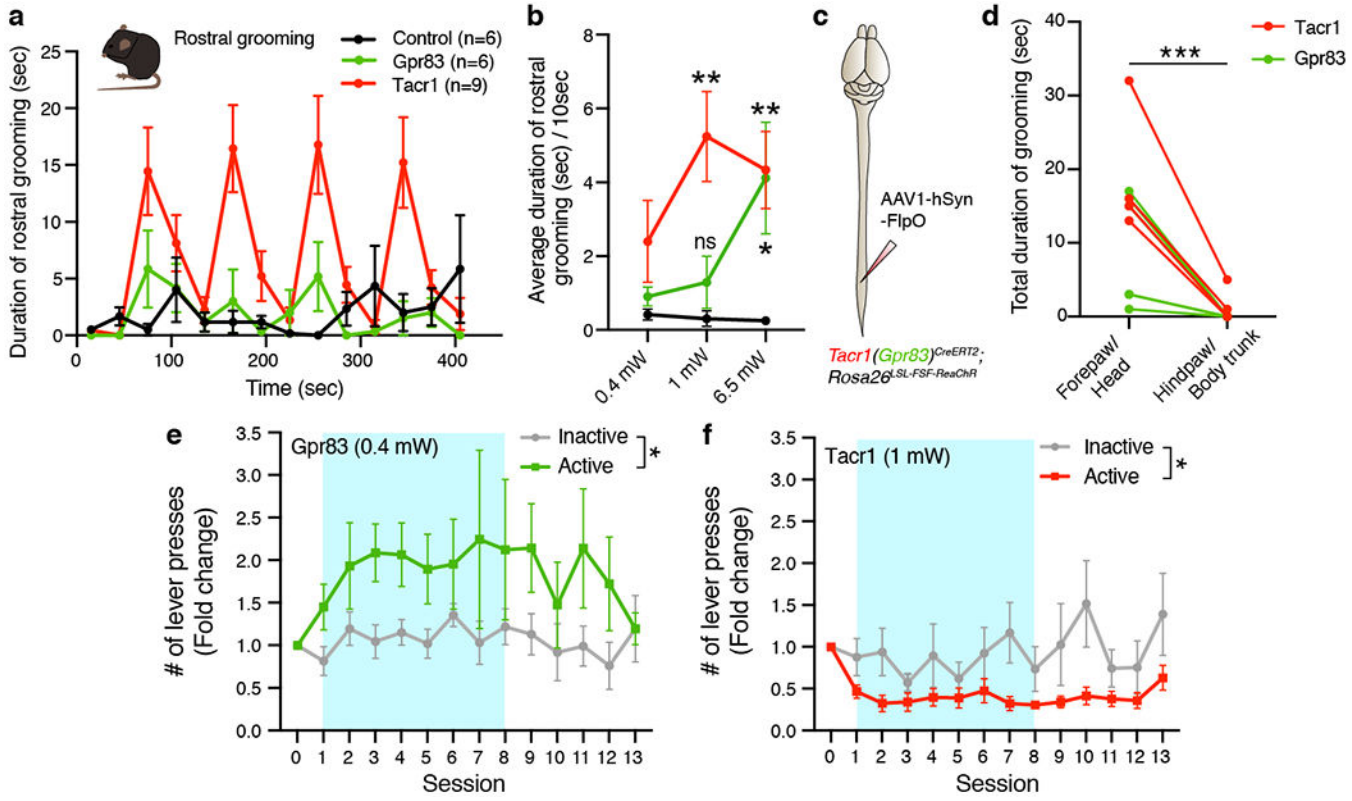

Extended Data Figure 9. Photostimulation of either *Tacr1*$^+$ or *Gpr83*$^+$ SPB neuron axon terminals promotes rostral grooming, and produces distinct behaviors in instrumental conditioning assays.

a, Duration of rostral grooming of control (black line), *Gpr83*^{CreERT2}; *Lbx1*^{FlpO}; *Rosa26*$^{LSL\text{-}FSF\text{-}ReaChR}$ (green line), or *Tacr1*^{CreERT2}; *Lbx1*^{FlpO}; *Rosa26*$^{LSL\text{-}FSF\text{-}ReaChR}$ (red line) mice over time. Bin size, 30 seconds. Axon terminals in the PBN_L were stimulated with blue LED (473 nm, 1 mW, 10 Hz, 10 ms pulse width) for 30 seconds 4 times (1 minute light-off periods between photostimulation periods). **b**, Quantification of average duration of rostral grooming during light-on periods for 0.4 mW, 1 mW, and 6.5 mW photostimulation. One-way ANOVA (Dunnett's multiple comparisons test); $F_{[2, 18]} = 7.60$ (1 mW), $F_{[2, 16]} = 7.49$ (6.5 mW); n = 6, 6, 9 mice (0.4 mW), 6, 7, 9 mice (1 mW), 8, 5, 6 mice (6.5 mW) for control, Gpr83, Tacr1, respectively. **c**, Schematic of lumbar injections of AAV1-hSyn-FlpO viruses. **d**, Quantification of total duration of grooming of different body parts during light-on periods. Axon terminals in the PBN_L were stimulated with blue LED (473 nm, 10 mW, 5 or 10 Hz, 10 ms pulse width) 4 times for 1 minute each (1 minute light-off periods between photostimulation periods). n = 4 trials (2 mice; 2 trials per mouse, 5Hz and 10 Hz stimulation) for *Tacr1*$^+$ SPB neuron terminal stimulation, n = 6 trials (3 mice; 2 trials per mouse, 5Hz and 10 Hz stimulation) for *Gpr83*$^+$ SPB neuron terminal stimulation. Paired *t*-test (two-tailed). **e**, Weak self-administered photostimulation (0.4 mW) of *Gpr83*$^+$ SPB neuron terminals led to an increase in the number of presses for the active lever, but not the inactive lever over time. **f**, Self-administered photostimulation (1 mW) of *Tacr1*$^+$ SPB neurons led to a decrease in the number of presses for the active lever, but not inactive lever over time. Turquoise boxes indicate 8 days of light-on sessions. n = 7 mice (Gpr83, 0.4 mW;

Tacr1, 1 mW). Two-way repeated measures ANOVA; $F_{[1, 6]} = 8.23$ (Gpr83, 0.4 mW), $F_{[1, 6]} = 9.43$ (Tacr1, 1 mW). Error bars, s.e.m.

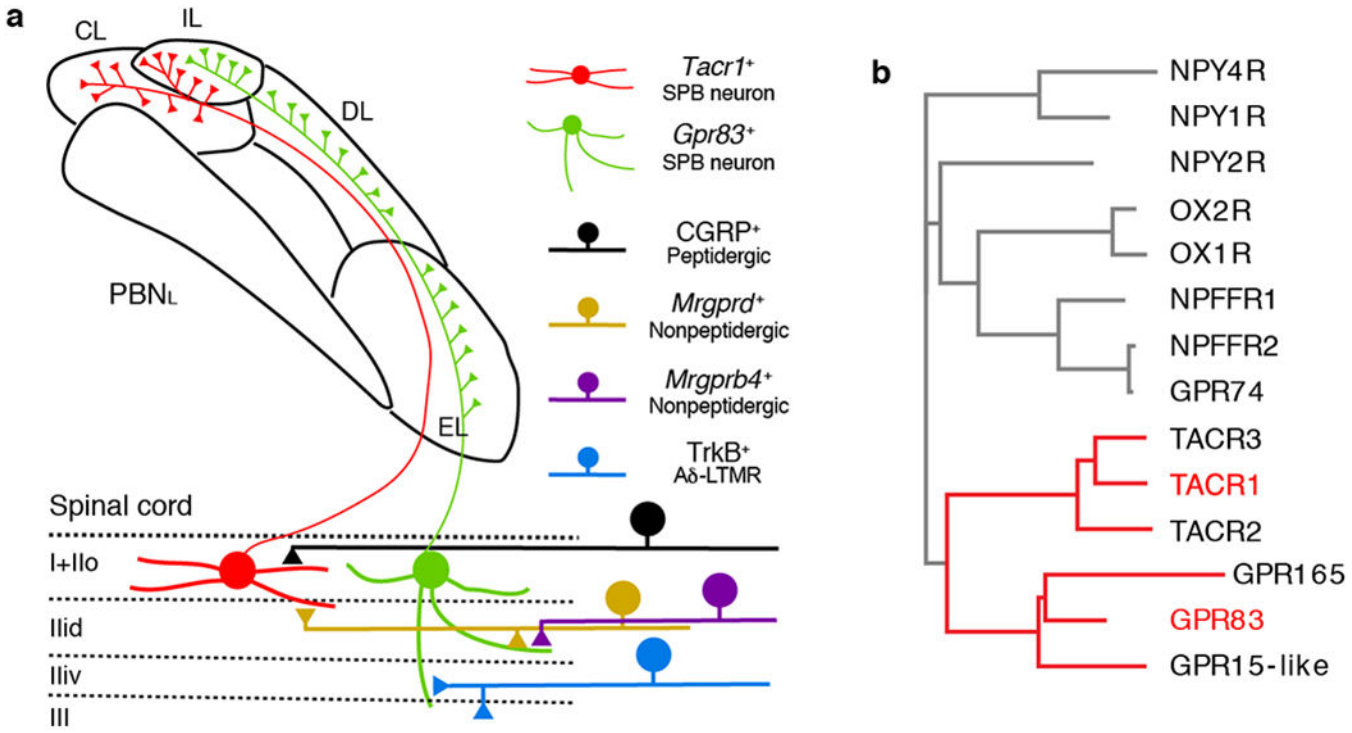

Extended Data Figure 10. Summary of two parallel ascending SPB pathways and a phylogenetic tree of structurally-related GPCR family proteins.

a, Summary cartoon of two parallel ascending SPB pathways for affective touch and pain. **b**, A phylogenetic tree generated using a multiple sequence alignment algorithm, ClustalW2 (EMBL-EBI). The top 14 mouse proteins that have the highest amino acid sequence similarity to mouse GPR83 were used for this analysis.

Supplementary Material

Refer to Web version on PubMed Central for supplementary material.

Acknowledgements

We thank all members of the Ginty laboratory for discussions and critical feedback during the course of the project. We thank David Paul and Clifford Woolf for feedback and critical evaluation of the manuscript, Susan Dymecki for providing *Rosa26*$^{LSL\text{-}FSF\text{-}TeTx}$ and *Rosa26*$^{FSF\text{-}LSL\text{-}SYN\text{-}GFP}$ mouse lines, LaTasha Crawford for help with initial characterization of the *Calca-FlpE* BAC transgenic mouse line, Travis Dickendesher for help with initial characterization of the *Advillin*^{FlpO} knockin mouse line, Connie Cepko for providing AAV1-FLEX-PLAP viruses, Silvia Arber for providing Cre-dependent AAV expression vector encoding synaptophysin-GFP, and Caiying Guo and the Gene Targeting and Transgenic Facility at the Janelia Research Campus of the Howard Hughes Medical Institute for generating mouse lines. We thank Bianca Kun, Maggie Streeter, Celine Breton, and Olivia Gabriel for their assistance with mouse husbandry, and histological and behavioral experiments. This work was supported by the Alice and Joseph E. Brooks Funds (S.C.), the Blavatnik Biomedical Accelerator Fund (S.C. and D.D.G.), NIH grants NS097344, NIH grant AR063772 (S.E.R.), NIH grant NS096705 (H.R.K.), NIH grant NS111643 (M.G.), the Bertarelli Foundation (D.D.G.), The Hock E. Tan and Lisa Yang Center for Autism Research at Harvard Univeristy (D.D.G.), and the Edward R. and Anne G. Lefler Center for Neurodegenerative Disorders (D.D.G). D.D.G. is an investigator of the Howard Hughes Medical Institute.

References

1. Abraira VE & Ginty DD The sensory neurons of touch. Neuron 79, 618–639, doi:10.1016/j.neuron.2013.07.051 (2013). [PubMed: 23972592]
2. Basbaum AI, Bautista DM, Scherrer G & Julius D Cellular and molecular mechanisms of pain. Cell 139, 267–284, doi:10.1016/j.cell.2009.09.028 (2009). [PubMed: 19837031]
3. Todd AJ Neuronal circuitry for pain processing in the dorsal horn. Nature reviews. Neuroscience 11, 823–836, doi:10.1038/nrn2947 (2010). [PubMed: 21068766]
4. Wercberger R & Basbaum AI Spinal cord projection neurons: a superficial, and also deep analysis. Current Opinion in Physiology 11, 109–115 (2019). [PubMed: 32864531]
5. Owens DM & Lumpkin EA Diversification and specialization of touch receptors in skin. Cold Spring Harb Perspect Med 4, doi:10.1101/cshperspect.a013656 (2014).
6. Haring M et al. Neuronal atlas of the dorsal horn defines its architecture and links sensory input to transcriptional cell types. Nat Neurosci 21, 869–880, doi:10.1038/s41593-018-0141-1 (2018). [PubMed: 29686262]
7. Gong S et al. A gene expression atlas of the central nervous system based on bacterial artificial chromosomes. Nature 425, 917–925, doi:10.1038/nature02033 (2003). [PubMed: 14586460]
8. Huang T et al. Identifying the pathways required for coping behaviours associated with sustained pain. Nature 565, 86–90, doi:10.1038/s41586-018-0793-8 (2019). [PubMed: 30532001]
9. Sabatier C et al. The divergent Robo family protein rig-1/Robo3 is a negative regulator of slit responsiveness required for midline crossing by commissural axons. Cell 117, 157–169, doi:10.1016/s0092-8674(04)00303-4 (2004). [PubMed: 15084255]
10. Bourane S et al. Gate control of mechanical itch by a subpopulation of spinal cord interneurons. Science 350, 550–554, doi:10.1126/science.aac8653 (2015). [PubMed: 26516282]
11. Abraira VE et al. The Cellular and Synaptic Architecture of the Mechanosensory Dorsal Horn. Cell 168, 295–310 e219, doi:10.1016/j.cell.2016.12.010 (2017). [PubMed: 28041852]
12. Palmiter RD The Parabrachial Nucleus: CGRP Neurons Function as a General Alarm. Trends Neurosci 41, 280–293, doi:10.1016/j.tins.2018.03.007 (2018). [PubMed: 29703377]
13. Fulwiler CE & Saper CB Subnuclear organization of the efferent connections of the parabrachial nucleus in the rat. Brain Res 319, 229–259, doi:10.1016/0165-0173(84)90012-2 (1984). [PubMed: 6478256]
14. Han S, Soleiman MT, Soden ME, Zweifel LS & Palmiter RD Elucidating an Affective Pain Circuit that Creates a Threat Memory. Cell 162, 363–374, doi:10.1016/j.cell.2015.05.057 (2015). [PubMed: 26186190]
15. Chiang MC et al. Divergent Neural Pathways Emanating from the Lateral Parabrachial Nucleus Mediate Distinct Components of the Pain Response. Neuron, doi:10.1016/j.neuron.2020.03.014 (2020).
16. Langford DJ et al. Coding of facial expressions of pain in the laboratory mouse. Nat Methods 7, 447–449, doi:10.1038/nmeth.1455 (2010). [PubMed: 20453868]
17. Craig AD, Krout K & Andrew D Quantitative response characteristics of thermoreceptive and nociceptive lamina I spinothalamic neurons in the cat. J Neurophysiol 86, 1459–1480, doi:10.1152/jn.2001.86.3.1459 (2001). [PubMed: 11535691]
18. Hachisuka J et al. Semi-intact ex vivo approach to investigate spinal somatosensory circuits. Elife 5, doi:10.7554/eLife.22866 (2016).
19. Bester H, Chapman V, Besson JM & Bernard JF Physiological properties of the lamina I spinoparabrachial neurons in the rat. J Neurophysiol 83, 2239–2259, doi:10.1152/jn.2000.83.4.2239 (2000). [PubMed: 10758132]
20. Andrew D Quantitative characterization of low-threshold mechanoreceptor inputs to lamina I spinoparabrachial neurons in the rat. J Physiol 588, 117–124, doi:10.1113/jphysiol.2009.181511 (2010). [PubMed: 19933757]
21. Liu Q et al. Molecular genetic visualization of a rare subset of unmyelinated sensory neurons that may detect gentle touch. Nat Neurosci 10, 946–948, doi:10.1038/nn1937 (2007). [PubMed: 17618277]

22. Li L et al. The functional organization of cutaneous low-threshold mechanosensory neurons. Cell 147, 1615–1627, doi:10.1016/j.cell.2011.11.027 (2011). [PubMed: 22196735]
23. Rau KK et al. Mrgprd enhances excitability in specific populations of cutaneous murine polymodal nociceptors. J Neurosci 29, 8612–8619, doi:10.1523/JNEUROSCI.1057-09.2009 (2009). [PubMed: 19571152]
24. Kalueff AV, Aldridge JW, LaPorte JL, Murphy DL & Tuohimaa P Analyzing grooming microstructure in neurobehavioral experiments. Nat Protoc 2, 2538–2544, doi:10.1038/nprot.2007.367 (2007). [PubMed: 17947996]
25. McGlone F, Wessberg J & Olausson H Discriminative and affective touch: sensing and feeling. Neuron 82, 737–755, doi:10.1016/j.neuron.2014.05.001 (2014). [PubMed: 24853935]
26. Foerster O, Breslau O, and Gagel O Die Vorderseitenstrangdurchschneidung beim Menschen: Eine klinisch-patho-physiologisch-anatomische Studie. Z. Gesamte Neurol. Psychiatr 138, 1–92 (1932).
27. Lahuerta J, Bowsher D, Campbell J & Lipton S Clinical and instrumental evaluation of sensory function before and after percutaneous anterolateral cordotomy at cervical level in man. Pain 42, 23–30, doi:10.1016/0304-3959(90)91087-y (1990). [PubMed: 1700355]
28. Hill R NK1 (substance P) receptor antagonists--why are they not analgesic in humans? Trends Pharmacol Sci 21, 244–246 (2000). [PubMed: 10871891]
29. Baseer N, Al-Baloushi AS, Watanabe M, Shehab SA & Todd AJ Selective innervation of NK1 receptor-lacking lamina I spinoparabrachial neurons by presumed nonpeptidergic Adelta nociceptors in the rat. Pain 155, 2291–2300, doi:10.1016/j.pain.2014.08.023 (2014). [PubMed: 25168670]
30. Gomes I et al. Identification of GPR83 as the receptor for the neuroendocrine peptide PEN. Science signaling 9, ra43, doi:10.1126/scisignal.aad0694 (2016). [PubMed: 27117253]
31. Hooks BM, Lin JY, Guo C & Svoboda K Dual-channel circuit mapping reveals sensorimotor convergence in the primary motor cortex. J Neurosci 35, 4418–4426, doi:10.1523/JNEUROSCI.3741-14.2015 (2015). [PubMed: 25762684]
32. Kim JC et al. Linking genetically defined neurons to behavior through a broadly applicable silencing allele. Neuron 63, 305–315, doi:10.1016/j.neuron.2009.07.010 (2009). [PubMed: 19679071]
33. Niederkofler V et al. Identification of Serotonergic Neuronal Modules that Affect Aggressive Behavior. Cell Rep 17, 1934–1949, doi:10.1016/j.celrep.2016.10.063 (2016). [PubMed: 27851959]
34. Zhou X et al. Deletion of PIK3C3/Vps34 in sensory neurons causes rapid neurodegeneration by disrupting the endosomal but not the autophagic pathway. Proc Natl Acad Sci U S A 107, 9424–9429, doi:10.1073/pnas.0914725107 (2010). [PubMed: 20439739]
35. Rutlin M et al. The cellular and molecular basis of direction selectivity of Adelta-LTMRs. Cell 159, 1640–1651, doi:10.1016/j.cell.2014.11.038 (2014). [PubMed: 25525881]
36. Vrontou S, Wong AM, Rau KK, Koerber HR & Anderson DJ Genetic identification of C fibres that detect massage-like stroking of hairy skin in vivo. Nature 493, 669–673, doi:10.1038/nature11810 (2013). [PubMed: 23364746]
37. Pivetta C, Esposito MS, Sigrist M & Arber S Motor-circuit communication matrix from spinal cord to brainstem neurons revealed by developmental origin. Cell 156, 537–548, doi:10.1016/j.cell.2013.12.014 (2014). [PubMed: 24485459]
38. Fenno LE et al. Targeting cells with single vectors using multiple-feature Boolean logic. Nat Methods 11, 763–772, doi:10.1038/nmeth.2996 (2014). [PubMed: 24908100]
39. Tervo DG et al. A Designer AAV Variant Permits Efficient Retrograde Access to Projection Neurons. Neuron 92, 372–382, doi:10.1016/j.neuron.2016.09.021 (2016). [PubMed: 27720486]
40. Lin JY, Knutsen PM, Muller A, Kleinfeld D & Tsien RY ReaChR: a red-shifted variant of channelrhodopsin enables deep transcranial optogenetic excitation. Nat Neurosci 16, 1499–1508, doi:10.1038/nn.3502 (2013). [PubMed: 23995068]
41. Lopes G et al. Bonsai: an event-based framework for processing and controlling data streams. Front Neuroinform 9, 7, doi:10.3389/fninf.2015.00007 (2015). [PubMed: 25904861]

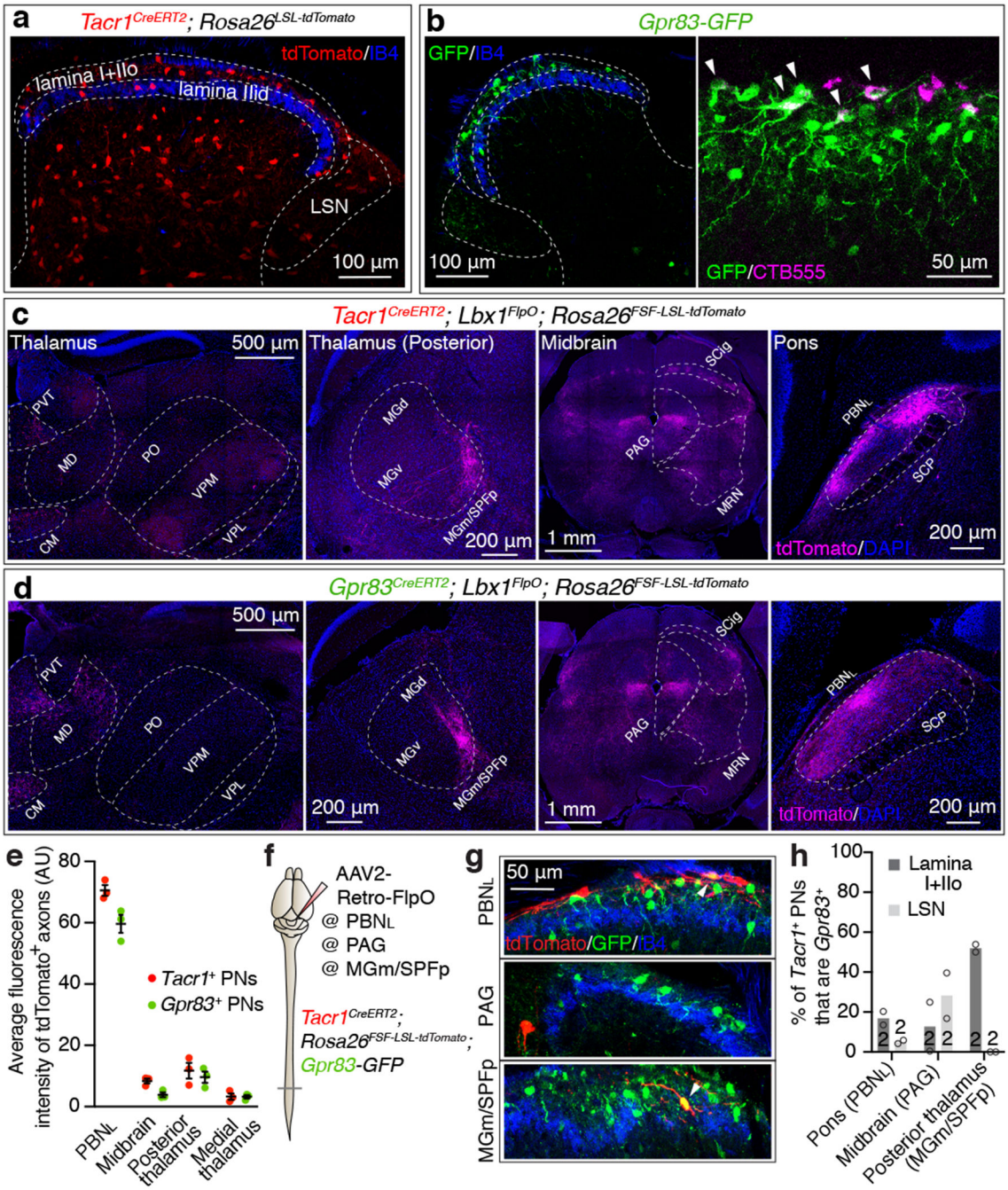

Figure 1. *Tacr1*- and *Gpr83*-expressing spinal PNs are largely distinct neuronal populations that innervate multiple distinct but overlapping brain regions.

a, Distribution of *Tacr1*$^+$ neurons in the spinal cord dorsal horn. IIo, outer lamina II; IIid, inner dorsal lamina II; LSN, lateral spinal nucleus. **b**, Distribution of GFP-expressing *Gpr83*$^+$ neurons in the spinal cord dorsal horn (left). A subset of SPB neurons labeled with CTB555 injected into the PBN_L are GFP-positive (right). Arrow heads, double-positive neurons. **c-d**, Axonal projections of *Tacr1*$^+$ or *Gpr83*$^+$ spinal PNs. PVT, paraventricular nucleus; CM, central medial nucleus; MD, mediodorsal nucleus; PO, posterior complex;

VPM, ventral posteromedial nucleus; MG(d)(v)(m), medial geniculate complex (dorsal) (ventral)(medial); SPFp, parvocellular subparafascicular nucleus; SCP, superior cerebellar peduncle. **e**, Quantification of the average fluorescence intensity of tdTomato-expressing *Tacr1*$^{+}$ and *Gpr83*$^{+}$ spinal PN axons in the major brain targets. n = 3 mice. Error bars, s.e.m. **f**, Schematic of virus injections for retrograde labeling of *Tacr1*$^{+}$ spinal PNs. **g**, Distribution of tdTomato-expressing *Tacr1*$^{+}$ spinal PNs and GFP-expressing *Gpr83*$^{+}$ neurons in the spinal cord dorsal horn. Arrowheads, double-positive neurons. **h**, Quantification of co-expression of tdTomato and GFP. n = number of mice (indicated in the bar graphs).

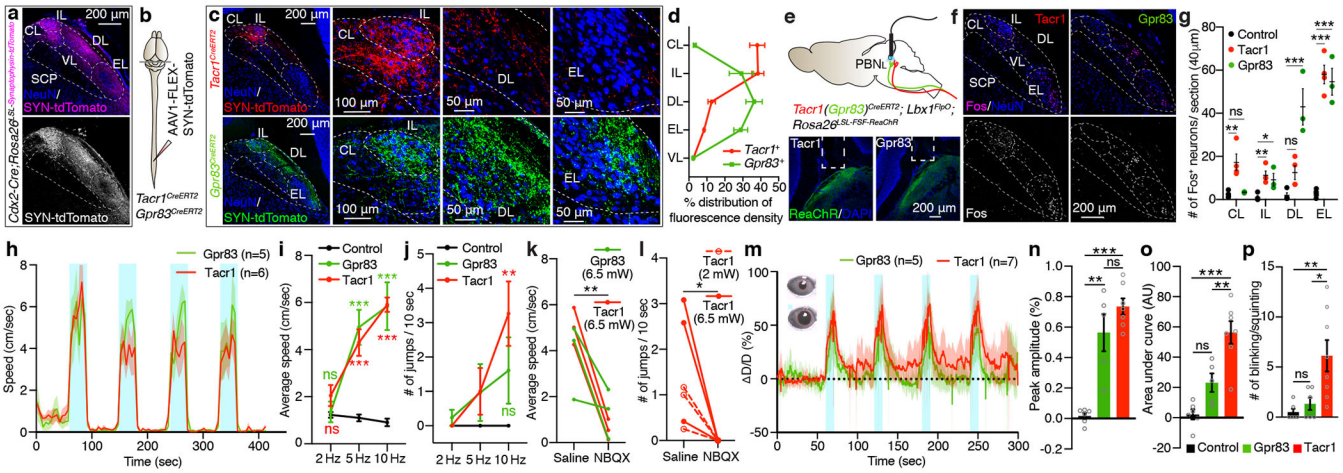

Figure 2. Axons of *Tacr1*- and *Gpr83*-expressing SPB neurons terminate in a zonally-segregated manner within the PBN_L and their strong activation produces distinct escape behaviors and autonomic responses.

a, Distribution of synaptic terminals originating from the spinal cord. n = 2 mice. **b**, Schematic of virus injections. **c**, Distribution of synaptic terminals of *Tacr1*$^+$ and *Gpr83*$^+$ SPB neurons in the PBN_L. **d**, Quantification. n = 5, 4 mice for *Tacr1*$^+$, *Gpr83*$^+$ SPB neurons, respectively. **e**, Top, schematic of optogenetic stimulation of SPB axonal terminals. Bottom, representative PBN_L images for fiberoptic implant sites. n = 5, 8 mice for *Tacr1*$^+$, *Gpr83*$^+$, respectively. **f**, Distribution of Fos$^+$ neurons in the PBN_L following high-power (6.5 mW) photostimulation. **g**, Quantification of the number of Fos$^+$ neurons in different PBN_L subnuclei. One-way ANOVA (Dunnett's multiple comparisons test); $F_{[2, 8]} = 11.70$ (PBN_{CL}), $F_{[2, 8]} = 8.58$ (PBN_{IL}), $F_{[2, 8]} = 21.21$ (PBN_{DL}), $F_{[2, 8]} = 63.00$ (PBN_{EL}); n = 4, 4, 3 mice for control, Tacr1, and Gpr83, respectively. **h**, Speed of movement over time. Turquoise bars, 30-second-long light-on periods (473 nm, 6.5 mW, 5 Hz, 10 ms pulse width). Shaded areas, s.e.m. **i**, **j**, Quantifications of average speed (i) and number of jumps (j) during light-on (6.5 mW) periods. One-way ANOVA (Dunnett's multiple comparisons test); $F_{[2, 16]} = 21.32$ (5 Hz), $F_{[2, 16]} = 31.05$ (10 Hz) (i); $F_{[2, 16]} = 6.53$ (10 Hz) (j); n = 8, 6, 5 mice for control, Tacr1, and Gpr83, respectively. **k**, **l**, Quantification of average speed (n) or number of jumps (o) during light-on (10 Hz) periods following NBQX (or saline) pre-infusion into the PBN_L. Paired *t*-test (two-tailed). **m**, Relative change in pupil diameter over time (ΔD/D, see methods for calculation). Inset, representative pupil images during baseline (top) and light-on (bottom) periods. Turquoise bars, 10-second-long light-on periods (473 nm, 2 mW, 10 Hz, 10 ms pulse width). Shaded areas, s.d. Note that abrupt downward lines in the shaded regions reflects blinking/squinting. **n-p**, Quantifications of peak amplitude (n), area under curve (o), and number of blinks/squints (p). One-way ANOVA (Tukey's multiple comparisons test); $F_{[2, 15]} = 30.44$ (peak amplitude), $F_{[2, 15]} = 21.11$ (area under curve), $F_{[2, 17]} = 7.412$ (blinks/squints); n = 6, 7, 5 mice for control, Tacr1, Gpr83, respectively. Error bars, s.e.m.

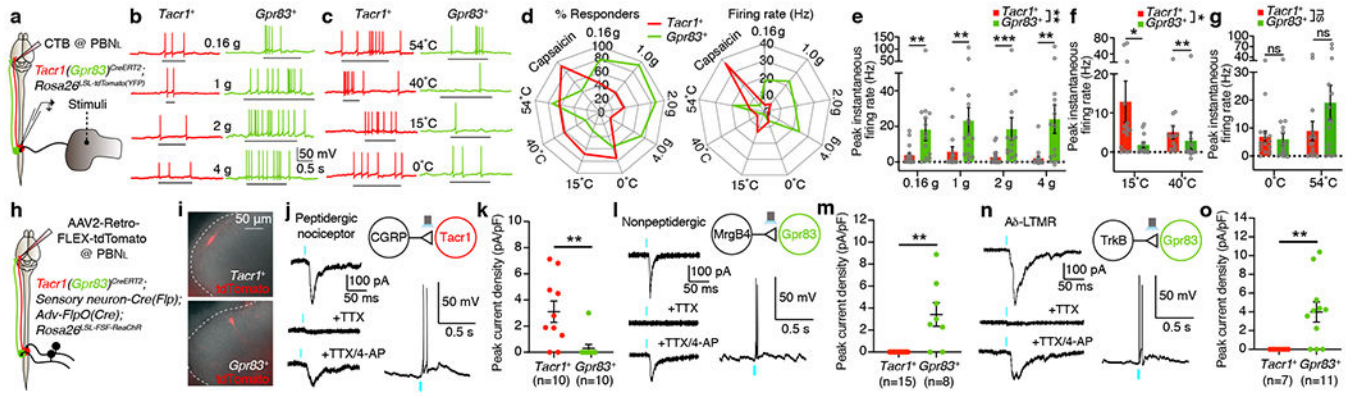

Figure 3. *Tacr1*- and *Gpr83*-expressing SPB neurons exhibit different responses to cutaneous stimuli, which is explained by their distinct synaptic inputs from primary sensory neuron subtypes.

a, Schematic of whole-cell patch clamp recordings from *Tacr1*$^+$ and *Gpr83*$^+$ SPB neurons using an *ex vivo* skin-spinal cord preparation. **b**, **c**, Representative traces of action potential (AP) firing evoked by von Frey filament indentations (b) and saline application with different temperatures (c). Underbars, time when stimuli were applied to the skin. **d**, Summary radar plots. **e-g**, Quantifications of peak instantaneous firing rates following application of mechanical (e) and temperature (innocuous (f) and noxious (g)) stimuli. Mann-Whitney test (two-tailed) (comparison for individual stimuli); Two-way ANOVA (comparison for different groups of stimuli), $F_{[1, 29]} = 9.77$ (e), $F_{[1, 57]} = 4.41$ (f); n = 16, 15 neurons for *Tacr1*$^+$, *Gpr83*$^+$, respectively. **h**, Schematic of whole-cell patch clamp recordings from *Tacr1*$^+$ and *Gpr83*$^+$ SPB neurons using a spinal cord slice preparation. The genetic labeling strategies are described in the methods. **i**, Representative images of tdTomato-expressing *Tacr1*$^+$ and *Gpr83*$^+$ SPB neurons in acute spinal cord slices. n = 39, 35 neurons for *Tacr1*$^+$, *Gpr83*$^+$, respectively. **j**, **l**, **n**, Representative traces of light-activated currents (left) and AP firing (right) upon photostimulation of CGRP$^+$ (j), *Mrgprb4*$^+$ (l), and *Ntrk2*$^+$ (n) primary afferent terminals. The light-activated EPSCs were abolished in the presence of tetrodotoxin (TTX) and reinstated in the presence of 4-aminopyridine (4-AP) in addition to TTX, indicating the monosynaptic nature of the synaptic connections. Turquoise bars, 0.1 ms (EPSCs) and 1 ms (APs) LED (473 nm) stimulations. **k**, **m**, **o**, Quantifications of peak current density. Mann-Whitney test (two-tailed); n = number of neurons. Error bars, s.e.m.

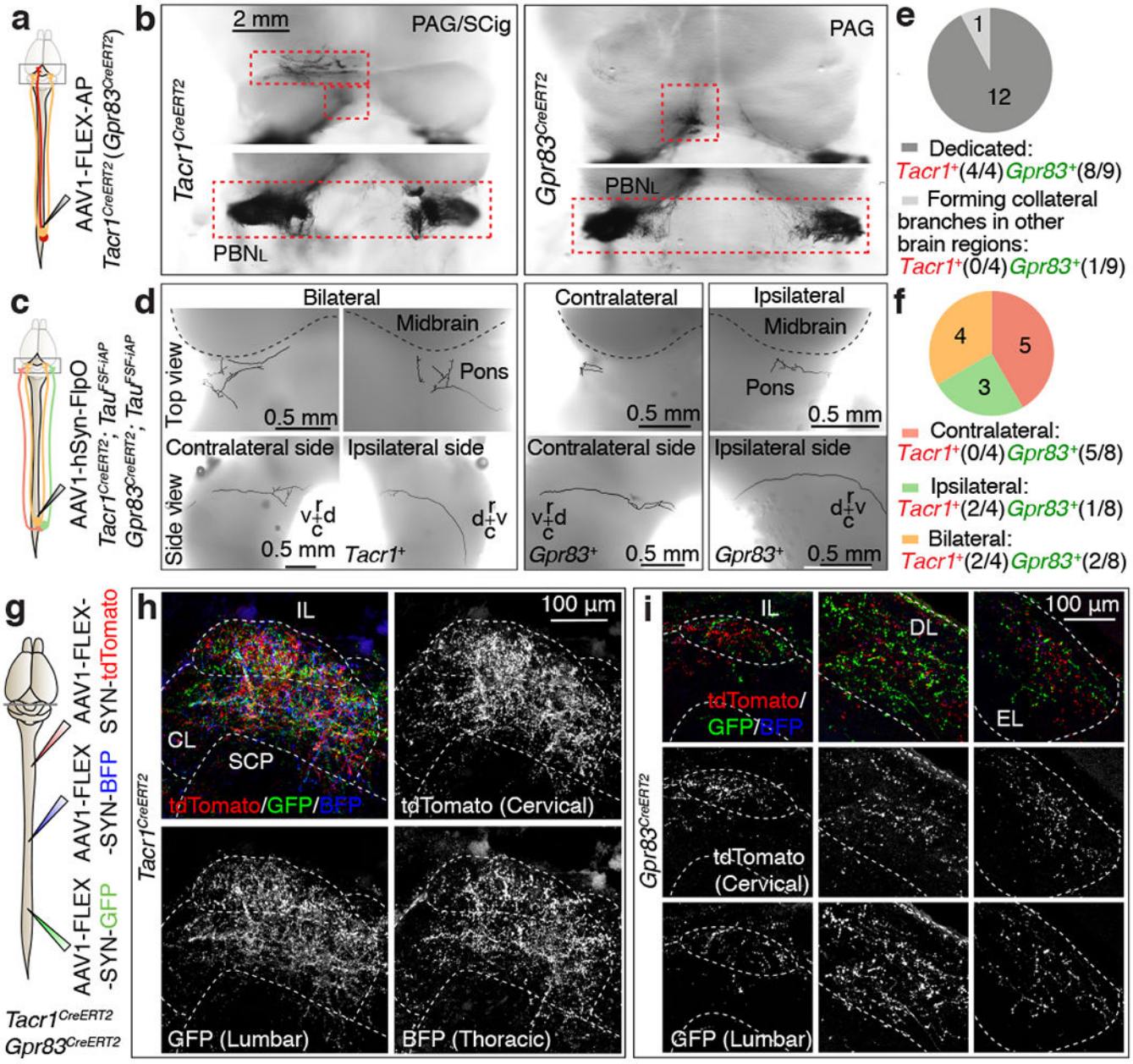

Figure 4. *Tacr1*- and *Gpr83*-expressing SPB neurons form dedicated, bilateral, non-somatotopically organized synaptic inputs to the PBN_L.

a, c, Schematics of unilateral lumbar injections of AAV viruses for whole-mount AP staining. **b**, Top view of whole-mount AP-stained axonal projections of densely labeled *Tacr1*$^+$ and *Gpr83*$^+$ spinal PNs. **d**, Single axon traces of sparsely labeled *Tacr1*$^+$ and *Gpr83*$^+$ SPB neurons. r, rostral; c, caudal, d, dorsal; v, ventral. **e, f**, Quantifications of the numbers of SPB neurons that exhibit dedicated vs. collateral-forming axons (e) and SPB neurons that innervate the PBN_L contralaterally, ipsilaterally, or bilaterally (f). **g**, Schematic of virus injections. **h**, **i**, Synaptic terminals of *Tacr1*$^+$ (h) or *Gpr83*$^+$ (i) SPB neurons representing hindlimb regions (GFP), thoracic body regions (BFP), and forelimb regions (tdTomato), are

intermingled within their respective PBN_L target subnuclei. n = 3 mice each for *Tacr1*$^+$ and *Gpr83*$^+$ SPB neurons.

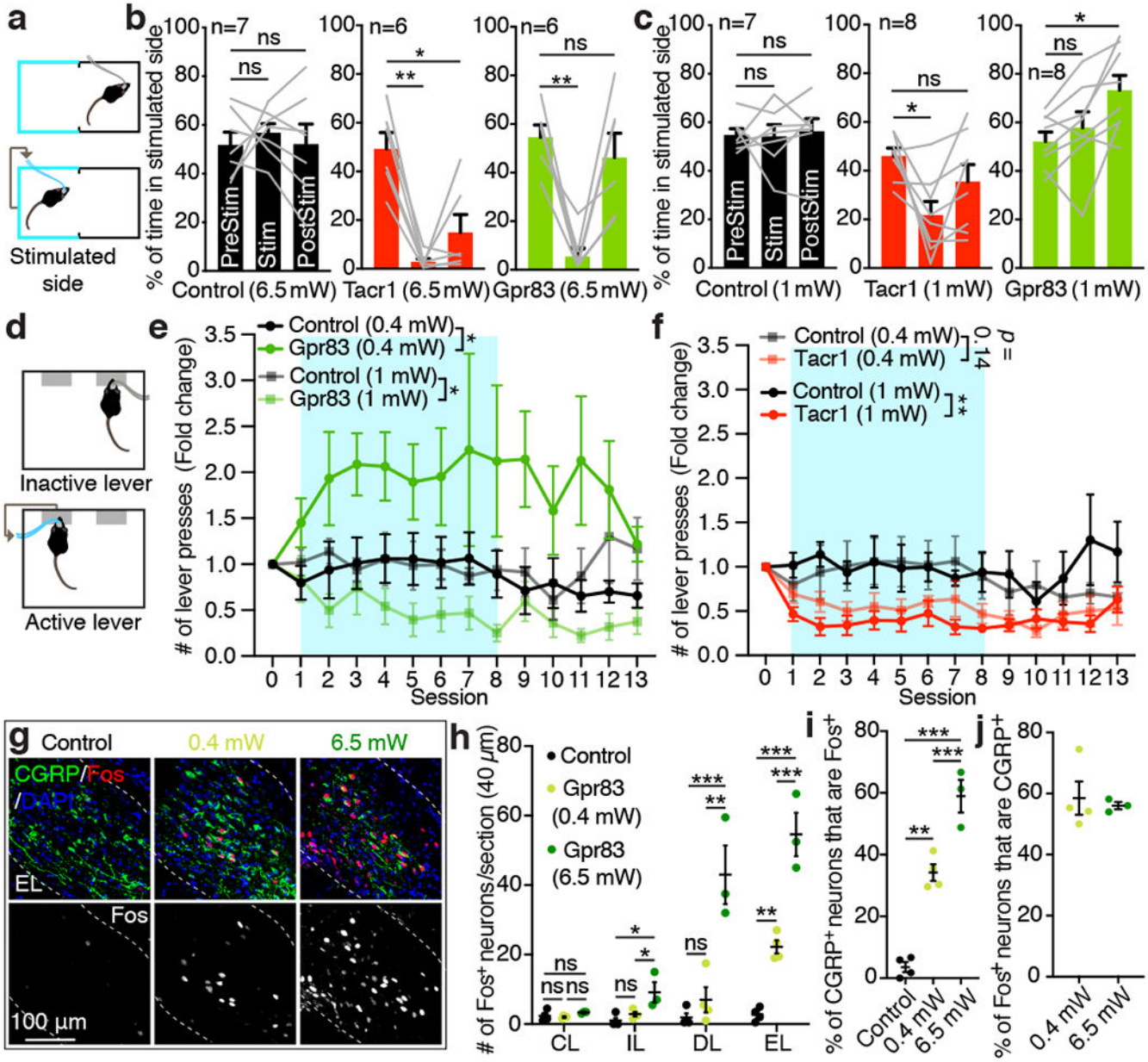

Figure 5. Activation of *Tacr1*- and *Gpr83*-expressing SPB neurons induces distinct affective behaviors in a stimulus intensity-dependent manner.

a, Schematic of the optogenetic stimulation-coupled real-time place preference assay. **b**, **c**, Quantifications of % of time spent in stimulated side for 6.5 mW (b) and 1 mW (c) photostimulations (10 Hz, 10 ms pulse width). One-way repeated measures ANOVA (Dunnett's multiple comparisons test); $F_{[1.626, 8.131]} = 19.10$ (Tacr1), $F_{[1.580, 7.901]} = 14.41$ (Gpr83) (b); $F_{[1.903, 13.32]} = 7.20$ (Tacr1), $F_{[1.817, 12.72]} = 8.42$ (Gpr83) (c); n = number of mice. **d**, Schematic of the optogenetic stimulation-coupled lever-pressing assay. Mice received 5 second-long photostimulation (473 nm, 10 Hz, 10 ms pulse width) upon pressing an active lever. **e**, **f**, Fold changes of number of lever press are plotted over sessions. Turquoise boxes, 8 days of light-on sessions. n = 7 (control, 0.4 mW; Tacr1, 0.4 mW; Gpr83,

0.4 mW; Tacr1, 1 mW), n = 6 (control, 1 mW), n = 8 mice (Gpr83, 1 mW). Two-way repeated measures ANOVA; $F_{[1, 12]} = 5.26$ (0.4 mW), $F_{[1, 12]} = 5.22$ (1 mW) (e); $F_{[1, 12]} = 2.50$ (0.4 mW), $F_{[1, 11]} = 10.14$ (1 mW). **g**, Distribution of Fos^+ neurons in the PBN_{EL} following photostimulation of *Gpr83*$^+$ SPB axon terminals. **h-j**, Quantifications of the number of Fos^+ neurons in different PBN_L subnuclei (h), % of $CGRP^+$ neurons that are Fos^+ (i), and % of Fos^+ neurons that are $CGRP^+$ (j). One-way ANOVA (Tukey's multiple comparisons test); $F_{[2, 8]} = 7.41$ (PBN_{IL}), $F_{[2, 8]} = 22.03$ (PBN_{DL}), $F_{[2, 8]} = 64.36$ (PBN_{EL}); $F_{[2, 8]} = 74.94$ (i); n = 4, 4, 3 mice for control, 0.4 mW, and 6.5 mW, respectively. Error bars, s.e.m.